Structure

Volume 26 Number 3 Pages 000–000 March 6, 2018

Structure

Volume 26
Number 3
March 6, 2018

www.cell.com

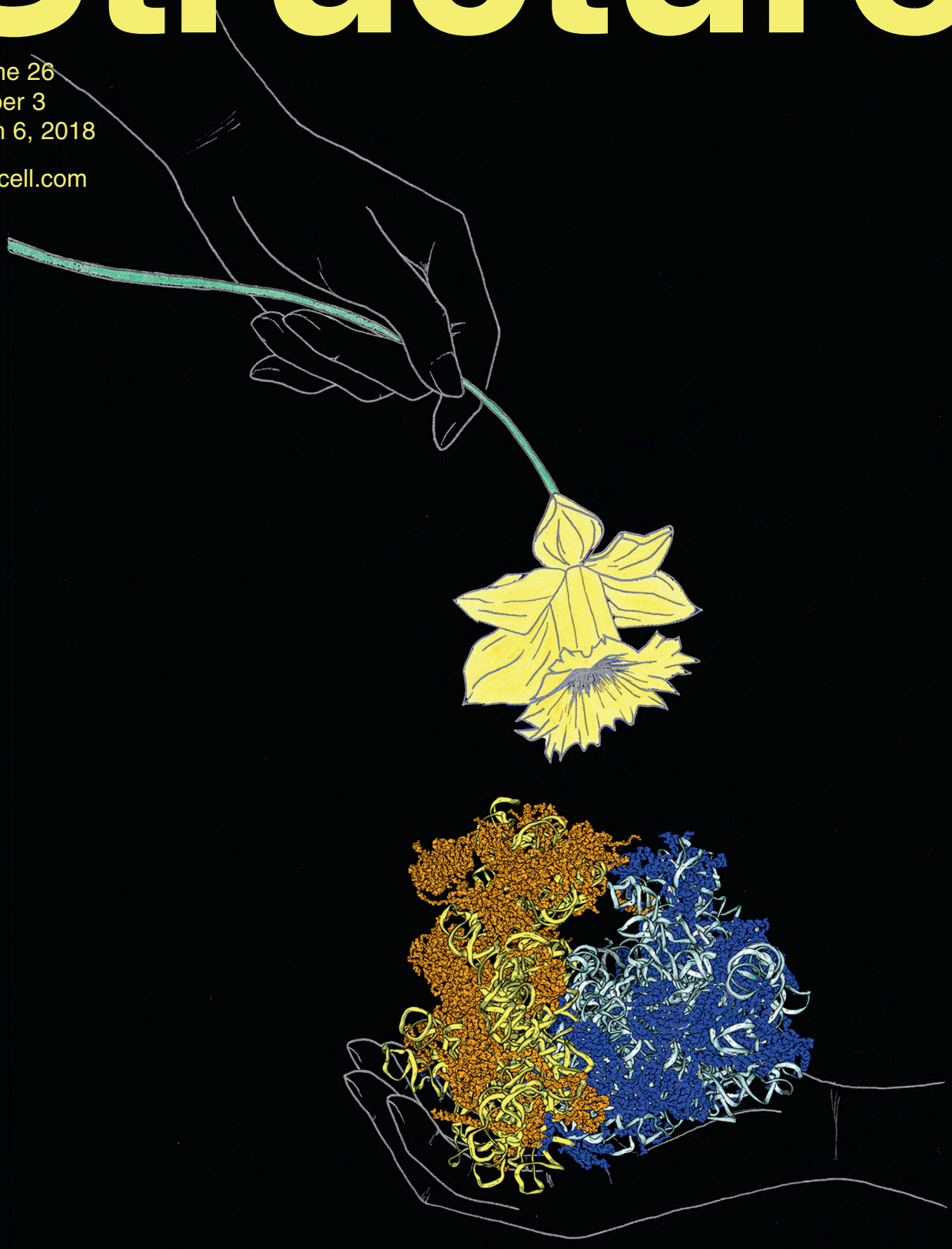

Article

Structure

The Amaryllidaceae Alkaloid Haemanthamine Binds the Eukaryotic Ribosome to Repress Cancer Cell Growth

Graphical Abstract

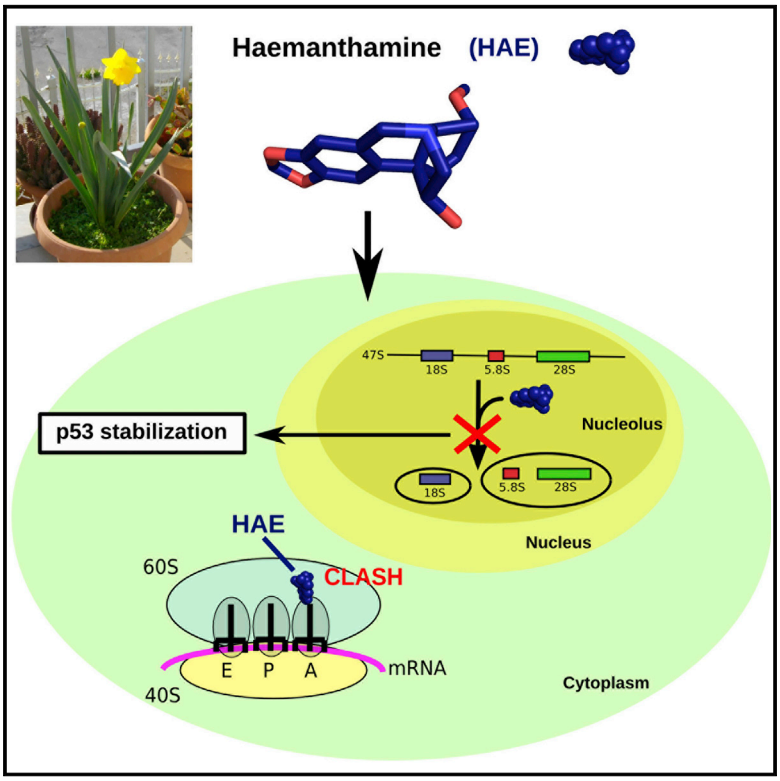

Highlights

- Anticancer drug haemanthamine binds to the A-site of the large ribosomal subunit
- Haemanthamine binding induces unique rRNA conformational rearrangements
- Haemanthamine and congeners specifically inhibit early stages of ribosome biogenesis
- Haemanthamine activates a p53-dependent antitumoral nucleolar stress response

Authors

Simone Pellegrino, Mélanie Meyer, Christiane Zorbas, ..., Alexander Kornienko, Denis L.J. Lafontaine, Marat Yusupov

Correspondence

denis.lafontaine@ulb.ac.be (D.L.J.L.), marat@igbmc.fr (M.Y.)

In Brief

Pellegrino, Meyer et al. map at atomic resolution the binding site of the Amaryllidaceae alkaloid haemanthamine onto the eukaryotic 80S ribosome, and demonstrate that it inhibits ribosome biogenesis and activates a p53-dependent antitumor pathway in cancer cells. They provide a structure-based rationale for designing more potent and less cytotoxic molecules.

Pellegrino et al., 2018, Structure *26*, 416–425
March 6, 2018
https://doi.org/10.1016/j.str.2018.01.009

CellPress

CellPress

Structure
Article

The Amaryllidaceae Alkaloid Haemanthamine Binds the Eukaryotic Ribosome to Repress Cancer Cell Growth

Simone Pellegrino,[1,7] Mélanie Meyer,[1,7] Christiane Zorbas,[2] Soumaya A. Bouchta,[2] Kritika Saraf,[2] Stephen C. Pelly,[3] Gulnara Yusupova,[1] Antonio Evidente,[4] Véronique Mathieu,[5] Alexander Kornienko,[6] Denis L.J. Lafontaine,[2,8,*] and Marat Yusupov[1,*]

[1]Institut de Génétique et de Biologie Moléculaire et Cellulaire (IGBMC), INSERM U964, CNRS UMR7104, Université de Strasbourg, 67404 Illkirch, France

[2]RNA Molecular Biology and Center for Microscopy and Molecular Imaging (CMMI), Fonds National de la Recherche (F.R.S./FNRS) and Université Libre de Bruxelles (ULB), BioPark Campus, 6041 Gosselies, Belgium

[3]Department of Chemistry and Polymer Science, Stellenbosch University, Stellenbosch, Matieland 7602, South Africa

[4]Dipartimento di Scienze Chimiche, Università di Napoli Federico II, Complesso Universitario Monte Sant'Angelo, Via Cintia 4, 80126 Napoli, Italy

[5]Laboratoire de Cancérologie et de Toxicologie Expérimentale, Faculté de Pharmacie, Université Libre de Bruxelles, 1050 Brussels, Belgium

[6]Department of Chemistry and Biochemistry, Texas State University, San Marcos, TX 78666, USA

[7]These authors contributed equally

[8]Lead Contact

*Correspondence: denis.lafontaine@ulb.ac.be (D.L.J.L.), marat@igbmc.fr (M.Y.)

https://doi.org/10.1016/j.str.2018.01.009

SUMMARY

Alkaloids isolated from the Amaryllidaceae plants have potential as therapeutics for treating human diseases. Haemanthamine has been studied as a novel anticancer agent due to its ability to overcome cancer cell resistance to apoptosis. Biochemical experiments have suggested that hemanthamine targets the ribosome. However, a structural characterization of its mechanism has been missing. Here we present the 3.1 Å resolution X-ray structure of haemanthamine bound to the *Saccharomyces cerevisiae* 80S ribosome. This structure reveals that haemanthamine targets the A-site cleft on the large ribosomal subunit rearranging rRNA to halt the elongation phase of translation. Furthermore, we provide evidence that haemanthamine and other Amaryllidaceae alkaloids also inhibit specifically ribosome biogenesis, triggering nucleolar stress response and leading to p53 stabilization in cancer cells. Together with a computer-aided interpretation of existing structure-activity relationships of Amaryllidaceae alkaloids congeners, we provide a rationale for designing molecules with enhanced potencies and reduced toxicities.

INTRODUCTION

Protein synthesis plays important roles in cancer onset and progression (Truitt and Ruggero, 2017). The high production rate of proteins in cancer cells, driven by its dysregulated control, makes the inhibition of the eukaryotic protein synthesis an attractive target for the development of anticancer agents (Bhat et al., 2015; Pelletier and Peltz, 2007). The ribosome is the protein-synthesizing factory inside each living cell. It is a large macromolecular complex made of rRNA and ribosomal proteins (~55 in bacteria, ~80 in eukaryotes) that is responsible for the correct translation of the information encoded in the mRNA into polypeptide chains. The ribosome is assembled in a sequential process during which ribosomal proteins are progressively recruited to the nascent pre-rRNAs and incorporated into maturing subunits. Recently it was shown that during subunit biogenesis, important sites on the ribosome, such as the decoding center and the exit tunnel, are monitored for integrity and function, sometimes on multiple events by different factors (Greber et al., 2016; Strunk et al., 2011; Wu et al., 2016). Loss of this tight regulation might lead to defective ribosome assembly and, by consequence, premature cell death (Wu et al., 2016). Inhibition of ribosome biogenesis is monitored by cells through activation of specific signaling cascades, including the antitumor nucleolar surveillance pathway leading to stabilization of the tumor-suppressor protein p53 (discussed in Nicolas et al., 2016). In normal cells, p53 is constitutively degraded by Hdm2-mediated ubiquitylation. In cells undergoing ribotoxic stress, unassembled ribosomal components capture Hdm2 and titrate it away from p53. As a result, p53 is stabilized and a cell death program is activated (Donati et al., 2013; Sloan et al., 2013).

Considering the central role of the ribosome in cell growth in the three kingdoms of life, it is not surprising that natural molecules have been selected during evolution as specific inhibitors of its function. Bacterial ribosome, for instance, has been shown to be the target of natural products synthesized by other bacteria or plants as part of self-defense mechanisms (Wilson, 2014). The eukaryotic ribosome, more importantly, is the target of the first eukaryotic protein synthesis inhibitor, omacetaxine mepesuccinate (homoharringtonine, Synribo®), isolated primarily from *Cephalotaxus harringtonii* and approved by the Food and Drug Administration (FDA) in 2012 for the treatment of chronic myeloid leukemia (Al Ustwani et al., 2014). Amaryllidaceae alkaloids

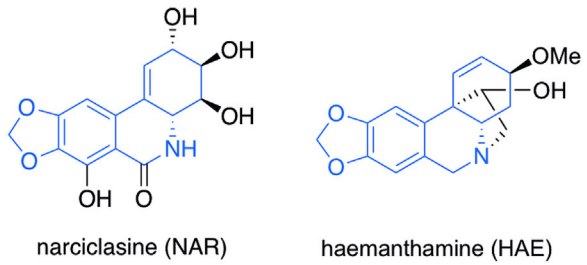

Figure 1. NAR and HAE Share a Common Methylenedioxy-Phenanthridine Skeleton

The two alkaloids belong to the Amaryllidaceae family of compounds and display chemical similarity. The common methylenedioxy-phenanthridine skeleton present in both structures is shown in blue.

(AAs) are a wide family of bioactive natural compounds used in folk medicine since the Greek and Roman ages for various purposes, including cancer treatment. Their biological activities are not restricted to anticancer effects but include potential anticholinesterase, antimalarial, antiviral, and anti-inflammatory effects (Furst, 2016; Sener et al., 2003). The most abundant alkaloids are galanthamine, lycorine (LYC), haemanthamine (HAE, Figure 1) and tazettine, together with the closely related isocarbostyryl narciclasine (NAR, Figure 1). Their isolation yields depend on the plant species, and the time and place of collection (Berkov et al., 2011; Lubbe et al., 2013). Galanthamine is an FDA-approved drug for the treatment of Alzheimer's disease due to its reversible and competitive inhibitory effects on the acetylcholinesterase, while other AAs, such as NAR or HAE, do not affect the activity of cholinesterases (Kukhanova et al., 1983). In contrast, NAR and HAE were originally suggested to share a common binding site on the eukaryotic ribosome and to specifically inhibit protein synthesis through their effects on peptide bond formation (Jimenez et al., 1976). At the same time NAR was shown to repress growth of S180 ascites tumors (Jimenez et al., 1976), revealing its potential as anticancer agent. We and others identified the crinine-type alkaloid HAE as a potential lead for anticancer drug development. Indeed, HAE exerts potent anticancer effects *in vitro* regardless of the sensitivity of cancer cells lines to apoptosis (Van Goietsenoven et al., 2010). Moreover, HAE is effective against multidrug-resistant cells and is not a substrate for the permeability glycoprotein (P-gp) efflux pump (Hohmann et al., 2002).

Although NAR is currently of great interest and is being pursued as a potential anticancer agent in several laboratories worldwide, a major drawback hampering its development is its poor water solubility (less than 100 μg/mL). From this perspective, HAE has a serious advantage as its water solubility is higher than 1 mg/mL and contains a basic nitrogen, allowing its potential administration in a salt form. A pharmacokinetic study of HAE in rats showed a rapid distribution phase of 30 min, a half-life of 70.4 min, and a major clearance through renal elimination (Hroch et al., 2016). The high distribution volume of 13.7 L/kg suggests a high intracellular penetration, and its plasmatic concentration remains higher than 1 μM for at least 1 hr after a single 10-mg/kg administration (Hroch et al., 2016). Because AAs, and HAE in particular, display several bioactivities, as mentioned above, the identification of the molecular target(s) and cellular pathways they inhibit, and the characterization of their mode of substrate binding are essential for the development of new AA-based drugs.

In this study, we solved the crystal structure of the alkaloid HAE in complex with the *Saccharomyces cerevisiae* 80S ribosome. We found that HAE binds at the A-site cleft of the peptidyl transferase center (PTC) on the large ribosomal subunit (LSU), creating unique molecular interactions with the 25S rRNA, which were not observed with related compounds such as NAR (Garreau de Loubresse et al., 2014). In addition, we discovered that four AAs, and in particular HAE, have a highly specific inhibitory effect on pre-rRNA processing, leading to the activation of a p53-dependent antitumoral surveillance pathway known as nucleolar stress (Pestov et al., 2001). This provides important insights into the mechanism of repression of cancer cell growth by AAs. Importantly, the processing inhibition and nucleolar stress activation were not seen in cells treated with cycloheximide (CHX), an unrelated potent inhibitor of ribosome function. Finally, we present a structure-activity relationship (SAR) discussion correlating the anticancer effects with the binding preferences of HAE analogs on the 25S rRNA of the ribosome.

RESULTS

HAE Binds to the A-Site Cleft of the PTC of the Eukaryotic Ribosome

As previously mentioned, it has been proposed that HAE halts protein biosynthesis by inhibiting the peptide bond formation (Jimenez et al., 1976). To validate these experimental results and gain further insights into the structural basis of inhibition, we solved the crystal structure of HAE in complex with the *S. cerevisiae* 80S ribosome at a maximal resolution of 3.1 Å (Table 1). Inspection of the unbiased electron density map ($F_{obs} - F_{calc}$) (Figure S1) revealed that the HAE binding site is located in the PTC on the LSU, and precisely in the pocket where the CCA end of the A-site transfer RNA (tRNA) is accommodated during the elongation phase (Figures 2A, 2B, and 3A). The difference map also revealed that only one molecule of HAE binds per ribosome, making the drug targeting highly specific. The binding pocket of HAE is very similar to that of NAR, whose structure in complex with the yeast 80S ribosome was recently solved (Garreau de Loubresse et al., 2014). Nonetheless, our structural analysis highlights remarkable differences in binding modes of HAE and NAR to the conserved 25S rRNA residues of the A-site cleft of the PTC (Figures 3A and 3B). HAE is sandwiched between the 25S rRNA residues U2875 and C2821, where the aromatic ring fused to the methylenedioxy moiety can form π-stacking interactions with the nucleotide bases (Figure 3A). Moreover, a hydrogen bond (H bond) is formed between the C=O4 carbonyl moiety of U2875 and the amino group of the purine G2403, stabilizing the "flip-up" conformation of the uracil residue (Figure 3A). Furthermore, HAE mediates the formation of two additional H bonds involving the C11-hydroxyl group (see Figure 4 for position numbering), one with the sugar-backbone moiety and the other with the C=O2 carbonyl moiety of the base of residue U2873. These might further stabilize the accommodation of HAE in the cleft and favor the binding of a supplementary Mg^{2+} atom, which was not detected previously (Ben-Shem et al., 2011; Garreau de Loubresse et al., 2014).

Table 1. Data Collection and Refinement Statistics

	HAE/80S Complex
Data Collection	
Space group	$P2_1$
Cell dimensions	
a, *b*, *c* (Å)	303.13, 286.50, 435.66
α, β, γ (°)	90.00, 98.87, 90.00
Resolution (Å)	100.00–3.10 (3.20–3.10)[a]
R_{meas} (%)	30.4 (223.4)
$I/\sigma I$	9.74 (1.36)
$CC_{1/2}$ (%)	99.3 (51.7)
Completeness (%)	99.5 (99.0)
Redundancy	7.48 (6.45)
Refinement	
Resolution (Å)	99.84–3.10
No. of reflections	1,317,535
R_{work}/R_{free}	0.2218/0.2520
No. of atoms	
Protein	178,889
RNA	222,512
Ions/ligands	8,947
B factors	
Protein	73.60
RNA	69.72
Ions/ligands	115.14
RMSDs	
Bond lengths (Å)	0.006
Bond angles (°)	0.935

Number of crystals used: 5. RMSD, root-mean-square deviation.
[a]Values in parentheses are for highest-resolution shell.

A comparison of our structure with the NAR/80S complex (PDB: 4U51, Figure 3B) reveals the structural rearrangement of the highly conserved residue U2875 on the 25S rRNA upon binding of HAE. Despite their related chemical structure (Figure 1), binding of NAR does not induce the "flip-up" conformation of U2875. It is likely that the phenolic hydroxyl present in NAR, but not in HAE, is engaged in H bonding with surrounding water molecules, which would lead to the loss of hydration energy upon forming a π-stacking interaction with U2875 (Figure 3B). A very similar reorganization of the 25S rRNA A-site cleft is also observed when we compared our structure with the yeast vacant 80S ribosome (PDB: 4V88, Figure S2A). In this case we additionally observed displacement of 25S rRNA residues C2821 and U2822, which accommodate HAE, similarly to what has been reported for the NAR/80S complex.

To expand our interpretation to ribosomes of higher eukaryotes, we performed structural superposition of the *S. cerevisiae* 25S rRNA (HAE/80S complex) with the 28S rRNA of the human 80S ribosome (PDB: 4UG0) (Figure 3C). The conserved residues forming the A-site cleft adopt a similar conformation, in which U4452 (U2875 in yeast) is found in an intermediate position between the vacant and HAE-bound yeast 80S ribosome (Figure 3C), suggesting that HAE is likely to bind human ribosome similarly.

Furthermore, using the obtained structure, we aimed to understand the reason why HAE is not effective against bacteria, although prokaryotic and eukaryotic ribosomes share a common functional core (Melnikov et al., 2012). In bacteria, U2822 is replaced by A2453, which could prevent the displacement seen in the HAE/80S structure compared with the vacant yeast 80S ribosome (Figure S2A). This mutation would not allow the conserved rRNA residue U2504 (U2873 in yeast) to adopt a conformation similar to that in the yeast ribosome. As a consequence, U2504 would clearly sterically clash with HAE, impeding its binding to bacterial ribosome (Figure S3A).

The Structure of HAE in Complex with the Eukaryotic 80S Ribosome Provides Rationalization of the Available Structure-Activity Relationships

The structure of HAE in complex with the eukaryotic 80S ribosome paves the way for the understanding of the SAR data *vis-à-vis* the anticancer activity of this and other crinine alkaloids. A comparative analysis of the antiproliferative activities of 56 crinine-type AAs related to HAE identified the relevant specific structural elements important for activity (Nair et al., 2012). These are represented with well-studied natural or synthetic molecules depicted in Figure 4. Examination of HAE and bulbispermine within the HAE binding pocket on the ribosome shows that the change in stereochemistry at C11 (as in bulbispermine Luchetti et al., 2012) or C3 (as in crinamine Likhitwitayawuid et al., 1993), would have very little impact: these functional groups protrude into a wide opening of the pocket, which can easily accommodate either stereochemistry (Figure 5A). A close HAE congener, haemanthidine (HAD), bearing a C6-hydroxyl, is virtually equipotent against all cancer cells studied (Hohmann et al., 2002; Van Goietsenoven et al., 2010). The C6-hydroxyl is not only well accommodated within the pocket, but may indeed be involved in additional hydrogen bonding to U2869 (Figure 5B). The derivatization of either of these alkaloids by acylating the C11-hydroxyl eradicates the activity regardless of the type of the acyl group (Cedron et al., 2015). Examination of acylated HAE in complex with the eukaryotic 80S ribosome reveals that there is no room in the binding pocket for derivatization of the C11-hydroxyl (Figure 5C). Lastly, the C11,C12-ethano bridge can be positioned α or β with respect to the tricyclic skeleton, and all β-ethano-bridge-containing alkaloids are virtually inactive as shown for bufanisine (Figure 4) (Likhitwitayawuid et al., 1993; Nair et al., 2012). These structures cannot adopt a conformation that is compatible with the binding pocket due to a serious steric clash with U2873 (Figure 5D). It should be noted that the active HAE congeners in Figure 4, i.e., haemanthidine, bulbispermine, and crinamine, retain the biological mechanism of action of HAE in that their antiproliferative action might result from the likely consequence of binding to the PTC A-site cleft as demonstrated here with HAE. Inhibition of protein synthesis was directly shown to be induced by crinamine (Novac et al., 2004), while haemanthidine (Nair et al., 2012) and bulbispermine (Luchetti et al., 2012) elicited cancer cell phenotypes similar to that of HAE, suggesting a common mechanism of action.

Effects of AAs on Ribosome Biogenesis

Pre-rRNA processing is an excellent proxy of ribosomal assembly, because failure to assemble r-proteins in a timely fashion

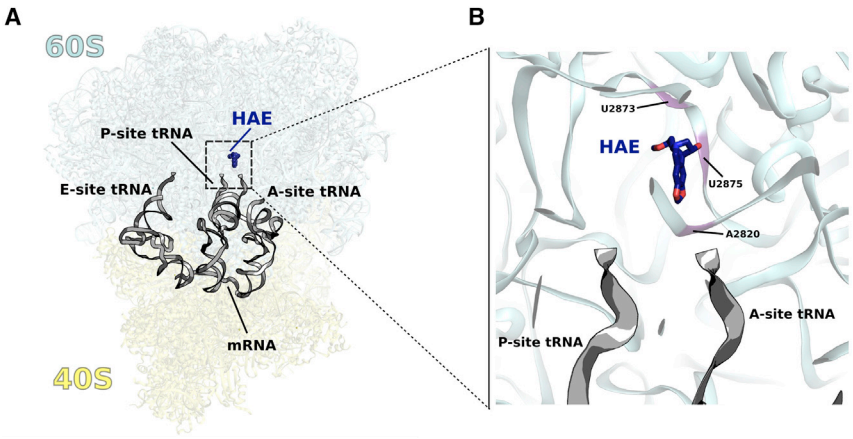

Figure 2. HAE Binds to the A-Site Cleft of the Large Ribosomal Subunit in the Eukaryotic Ribosome

(A) Cartoon representation of the *S. cerevisiae* 80S ribosome structure, showing the binding site of the inhibitor HAE. The three tRNAs and the mRNA (outlined in gray) have been modeled *in silico* upon superposition of our structure with the *Thermus thermophilus* 70S ribosome (PDB: 4V5D) to mimic an actively elongating ribosome.

(B) Zoom-in of the functional sites of the 80S ribosome, exhibiting where HAE interacts within the A-site cleft of the 25S rRNA. The residues involved in making direct contacts with HAE (U2873, U2875, and A2820) are colored violet on the 25S rRNA (cyan ribbon). Modeled A- and P-site tRNAs are shown as outlines for reference.

See also Figure S1.

during subunit biogenesis usually leads to inhibition of RNA cleavage (discussed in Wu et al., 2016). Three out of four human rRNAs are produced from a single polycistronic precursor synthesized by RNA polymerase I, the 47S pre-rRNA, by extensive processing (see Figures S4A and S4B). In untreated cells, the 47S is rapidly processed (at sites 01, 02, A0, and 1, see Figure S4A), so it is detected only at low levels (Figure 6A, 0-hr time point). Inhibition of early processing reactions leads to 47S accumulation. Typically, this is seen after treatment of cells with the anticancer agent 5-fluorouracil (5-FU), a nucleotide analog that inhibits rRNA synthesis and the downstream processing steps leading to ribosome biogenesis inhibition and translational remodeling (Figure 6A, and see Nicolas et al., 2016; Strunk et al., 2011). We were intrigued to test whether AAs have a direct effect on pre-rRNA processing, since the PTC is assembled in the early steps of the process.

We performed total RNA extraction from cells treated with a selection of compounds in a time-course analysis and identified the major pre-rRNA intermediates (Figures 6A and S4C). We chose to treat cells separately with each of four AAs that bind to the A-site cleft: LYC, HAE, HAD, and NAR. For comparison, we treated cells with CHX, an E-site binder. All compounds were used in the range of their half-maximal inhibitory concentration (IC_{50}) (Ingrassia et al., 2008; Lamoral-Theys et al., 2009; Myasnikov et al., 2016; Nita et al., 1998; Pettit et al., 2004; Van Goietsenoven et al., 2010). We observed different effects on early processing (47S accumulation readout). CHX treatment did not seem to affect early processing considerably (no significant 47S accumulation), but all four AAs tested did so to some extent (47S accumulation). The strongest effects were observed after HAE or HAD treatments (Figure 6A, see quantification). In more detail, pre-rRNA processing analysis revealed further differences in processing inhibition according to the type of compound used (Figure S4C). 5-FU treatment affected primarily the early steps of processing (cleavages at sites 01, 02, A0, and 1, as seen by the accumulation of the 47S, 34S, 30S, and 26S RNAs). It also affected, to a lesser extent, processing in the internal transcribed spacers 1 (ITS1, reduction of 21S/21S-C) and 2 (ITS2, reduction of 32S and 12S) (Figure S4C). Treatment with CHX affected only cleavage at site 2 in ITS1 (30S and 21S reduction), and the effect was marginal. In addition to strongly affecting the early processing steps of the primary transcript (47S accumulation), all four AAs tested specifically inhibited large ribosomal subunit formation. Processing in ITS2, which separates the coding sequences of the 5.8S and 28S rRNAs (Figures S4A and S4B), was particularly affected, as seen by the strong accumulation of 32S RNA (inhibition of cleavage at site 3′) and 12S RNA (inhibition of maturation at site 4). In conclusion, all four AAs tested exert similar and highly specific inhibitions on pre-rRNA processing which, strikingly, are different to those caused by another translation inhibitor (CHX) or another compound that inhibits rRNA synthesis (5-FU). Note that wild-type yeast cells are resistant to HAE even to doses 10-fold higher than those used in human cells, and therefore pre-rRNA processing was not tested in this model organism (Figure S6).

HAE and HAD Promote Substantial p53 Stabilization in Colon Carcinoma Cells

Cancer cells are particularly sensitive to a reduction in protein synthesis. This makes protein synthesis inhibitors promising cytostatic agents in cancer therapy (Truitt and Ruggero, 2017). We reasoned that if, in addition to impairing translation, HAE and other AAs triggered a nucleolar stress response leading to p53 stabilization, it would make them more effective anticancer agents. Effects on protein synthesis, ribosome biogenesis, and p53 stabilization would all contribute to preferential killing of cancer cells. We were particularly interested in learning whether the processing phenotypes caused by cell treatment with AAs trigger nucleolar stress activation and an increase in the p53 steady-state level. This was tested in a time-course analysis by western blotting with an anti-p53 antibody (Figures 6B and 6C). As loading controls, the blots were probed for several stable long-lived proteins: β-actin (a cytoskeleton protein), SP1 (a transcription factor), and GAPDH (a housekeeping metabolic enzyme) (Figures 6B and S5). By comparison with 5-FU treatment, which causes a 4-fold increase in the steady-state level of p53, incubating cells with CHX led to a gradual decrease in the p53 level, in agreement with the expected gradual reduction in protein synthesis after CHX treatment. To some extent, a similar trend (gradual reduction) was observed after treatment with the AAs LYC and NAR. After treatment with HAE or HAD, in contrast, the level of p53 remained elevated throughout the

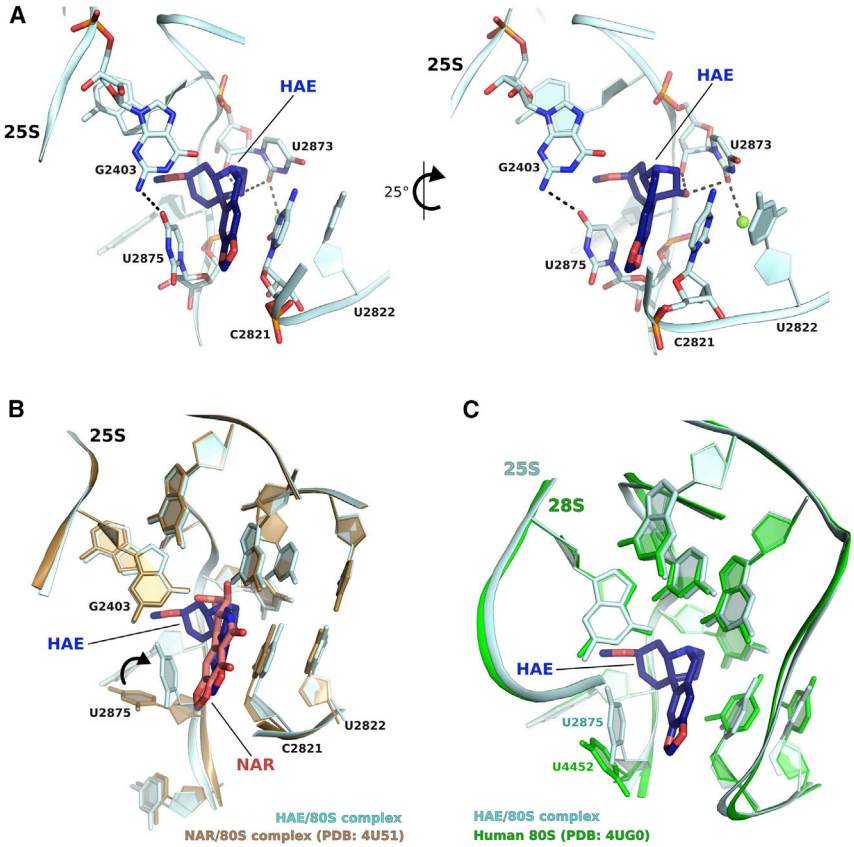

Figure 3. HAE Binding Is Mediated by Unique Interactions with the 25S rRNA

(A) HAE binds exclusively to rRNA residues in the PTC A-site on the LSU. Two views are presented, 25° apart, to show the interactions involved upon binding of HAE into the pocket. A π-stacking interaction is formed between the aromatic ring of HAE and the pyrimidine C2821, as seen previously upon NAR binding to the same region. However, HAE induces the "flip-up" rearrangement of the conserved residue U2875 and creates an additional hydrogen bonding with U2873, which represents a distinctive feature within the class of alkaloid inhibitors. The "flip-up" conformational change might further stabilize the inhibitor in the pocket and allow the binding of an Mg^{2+} atom to residue U2873 that may be involved in coordination of the neighboring rRNA residues.

(B) Comparison of HAE/80S structure with NAR/80S (PDB: 4U51) complex reveals that the "flip-up" rearrangement of residue U2875 is uniquely promoted by HAE binding to the A-site cleft. The accommodation of the two inhibitors does not induce further conformational changes in the pocket, except the stabilization of an Mg^{2+} atom in the close proximity of the C11-hydroxyl group of HAE.

(C) Structural superposition of the A-site cleft of the human 28S rRNA (PDB: 4UG0) with the structure presented in this study. The overall conformation is very similar and we can observe an intermediate position of residue U4452 (U2875 in yeast), which can likely allow the accommodation of the inhibitor, thus confirming that the model we present is highly supportive of the biological data produced so far. See also Figures S2 and S3.

depletion time course (see quantification, Figure 6C). In these cases, p53 thus appears to be stabilized by nucleolar stress activation. Consistent with these results, the processing phenotypes caused by treatment with HAE or HAD are much stronger than those observed with the other two alkaloids tested (1,652% and 1,071% 47S accumulation after HAE or HAD treatment, respectively, versus only 450% and 206%, respectively, after NAR or LYC treatment) (Figures 6A and S4C). This suggests that a certain threshold of processing inhibition needs to be passed in order to trigger nucleolar stress activation.

Impedimetric Measurements Reveal Cancer Cell Sensitivity to AAs

To gain further insights into the effects of AAs in cancer cells, we monitored cell adhesion by real-time electric impedance measurements (Figure 6D). The same number of colon carcinoma cells were seeded into each well of gold-plated microtiter plates, and the impedance was measured every 10 min for up to 3 days. The different compounds were added once the cells were properly attached to the support (Figure 6D, red arrow). Over the first 5 hr of treatment, addition of 5-FU, CHX, or vehicle alone (DMSO, mock) led to an initial mild reduction of cell adhesion (adhesion rate below 0 after 30 min), followed by gradual recovery. It took about 5 hr of CHX treatment to affect growth clearly, while 5-FU did not seem to have much effect within this time frame. Strikingly, the four AAs displayed distinct, but consistent, effects: after an initial increase, the cell adhesion rate started to decrease rapidly, reaching a below-zero level and growth inhibition after 2–3 hr of treatment, i.e., sooner than upon CHX treatment (5 hr). This observation is consistent with the idea that the AAs may kill cancer cells more effectively than drugs that inhibit only protein synthesis (CHX) or ribosome biogenesis (5-FU).

To prove that the effects on growth of compounds that trigger nucleolar stress require the presence of p53 in cells, we monitored cell proliferation by impedance measurements after treatment with 5-FU or HAE (both elicit p53 stabilization, Figures 6B and 6C) in two isogenic diploid human cancer cell lines: one expressing p53 (HCT116 $p53^{+/+}$) and one not expressing p53 (HCT116 $p53^{-/-}$) (Figure S7). As controls, cells were treated with CHX (which does not lead to p53 stabilization, Figures 6B and 6C) or the vehicle alone (DMSO). In agreement with the nucleolar stress activation model (discussed in Nicolas et al., 2016), cells treated with 5-FU are more rapidly and more severely affected for growth if they express p53 than if they do not (Figure S7). Similarly, upon HAE treatment, $p53^{-/-}$ cells grow better than $p53^{+/+}$ cells. The range of effects on growth upon 5-FU and HAE treatment is consistent with the extent of p53 stabilization: strong with 5-FU and moderate with HAE (see Figures 6B–6D). By comparison, CHX similarly affects cells growth independently of their p53 status (Figure S7). In conclusion, the reported p53 stabilization reflecting nucleolar stress activation and ribosome biogenesis inhibitions is physiologically impactful.

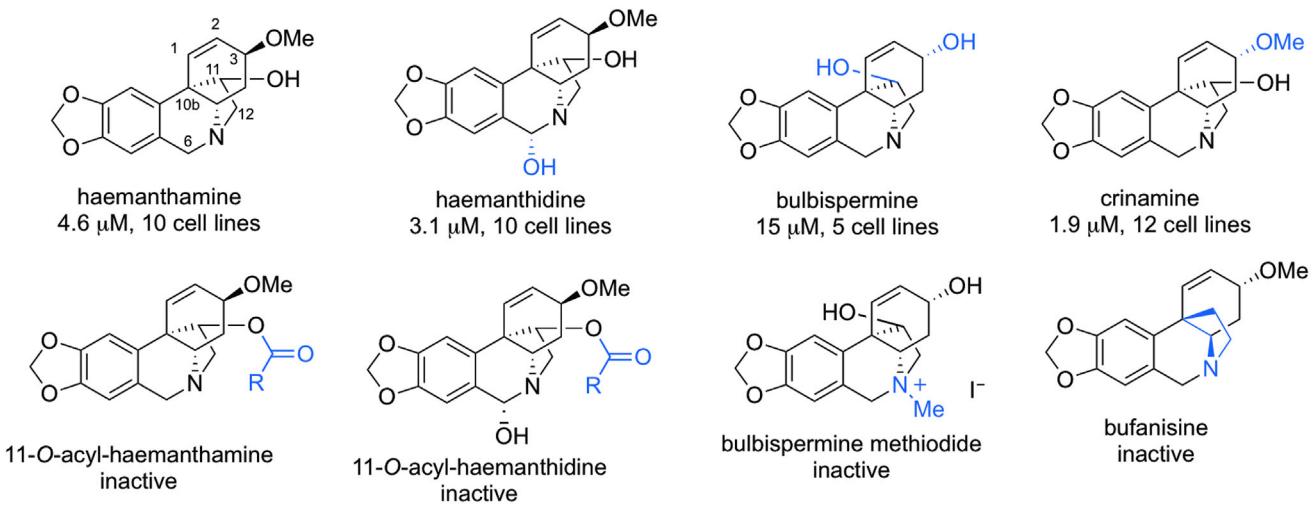

Figure 4. Representative HAE-Related Natural and Synthetic Molecules Illustrate the Structure-Activity Relationship in This Series of Compounds

For position numbering, see the structure of HAE. The structural variations from HAE are indicated in blue. Reported for each compound are also cytotoxicity data measured as IC_{50} values, together with the number of cell lines tested.

DISCUSSION

AAs are potent anticancer drugs that target the eukaryotic ribosome by inhibiting protein synthesis (Jimenez et al., 1976; Garreau de Loubresse et al., 2014). Here we have extended this conclusion to haemanthamine by mapping its binding site on the ribosome at atomic resolution (Figures 2 and 3). The crystal structures of LYC and NAR, members of this family, in complex with the *S. cerevisiae* 80S ribosome have recently revealed that their target is the A-site cleft located at the PTC on the LSU (Garreau de Loubresse et al., 2014). HAE, a crinine-type alkaloid, also belongs to the AA family, but has the substantial advantage of being soluble in water at higher concentration, making it a better candidate for future preclinical studies. Hence we were particularly interested in solving the crystal structure of HAE in complex with the eukaryotic 80S ribosome. Because HAE and NAR are both based on the methylenedioxy-phenanthridine scaffold, they were expected to share binding site and, indeed, we observed that HAE also binds to the A-site on the LSU. However, there was evidence from studies conducted in the 1970s that distinct members of the AAs display differential *in vitro* ribosome binding and differential *in vitro* translation inhibition (Baez and Vazquez, 1978). While this suggested that individual members of the family may adopt specific modes of interaction with the ribosome, the rationale for these differences remained unknown for 50 years. One possibility is that the different compounds bind differently to the ribosomal A-site cleft. This is indeed what we confirmed here for HAE by our X-ray structural studies (see Figure S2B and Garreau de Loubresse et al., 2014). Our crystal structure highlights the noticeable rearrangement of the conserved rRNA residue U2875 upon binding of HAE to the 80S ribosome. We observed a ~75° displacement of the base toward the inhibitor ("flip-up") to establish a stacking interaction with it (Figure 3A). Moreover, we detected the formation of an additional H bond with residue U2873, which was not detected in the case of NAR binding (Figure 3), which could further stabilize the alkaloid in the pocket. Superposition of our structure with the 28S rRNA of the human 80S structure (PDB: 4UG0) highlights the high similarity of the A-site cleft, further validating our interpretation of the HAE binding mode (Figure 3C).

The first step of the elongation phase in protein translation, after the initiator tRNA has been recognized and the 80S fully assembled, is the loading of the correct aminoacylated-tRNA (aa-tRNA) in the A-site, dictated by the mRNA sequence. The crystal structure of *Thermus thermophilus* 70S ribosome containing aa-tRNAs in the A and P-sites revealed the interactions occurring at the PTC between the 23S rRNA and the CCA-end tails of tRNAs (Voorhees et al., 2009). Contacts of the rRNA residues located at the PTC A-site take place mainly with the amino acid backbone, which makes the mechanism universal for all of the 20 different amino acids. The superposition of this structure onto our model led us to speculate that, in eukaryotes, the mechanism of inhibition occurs via a steric clash of the aa-tRNA with the alkaloid (tRNAs taken from PDB: 4V5D). The drug is placed at a distance of approximately 3 Å from the amino acid backbone and blocks the access of bulky or long side chains in the A-site cleft (Figure S3A), thereby hindering peptide bond formation through rejection of the aa-tRNA. Steric clash interference is a mechanism of inhibition used by many protein synthesis inhibitors that bind to the functional sites of the mature ribosome (Garreau de Loubresse et al., 2014; Könst et al., 2017; McClary et al., 2017; Wilson, 2014).

By comparison with its bacterial counterpart, the eukaryotic ribosome has become more complex during evolution (Melnikov et al., 2012). This higher complexity is concentrated at the surface of the ribosome, with the addition of several ribosomal proteins and rRNA expansion segments, while the functional sites located at the core of the ribosome, such as the PTC, have maintained a high level of conservation both in sequence and structure (Melnikov et al., 2012). This is also the case for the A-site

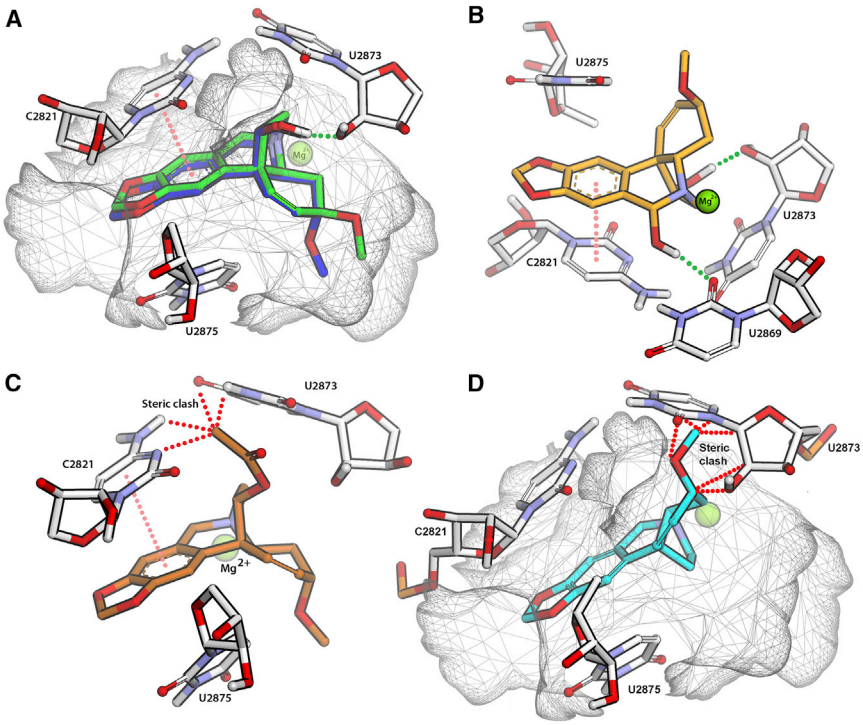

Figure 5. Molecular Docking based on the HAE/80S Structure Allowed Us to Better Understand the SAR Data

(A) Representation, using a wire mesh surface, of the extent of the A-site binding pocket based on the HAE/80S crystal structure obtained in this study (HAE in dark blue). Significant interactions include π-stacking to C2821 and hydrogen bonding to U2873 (green dotted line). The superimposition of crinamine (green) onto HAE shows that the alternative stereochemistry at C3 is well accommodated within the constraints of the binding pocket.

(B) HAD (orange) within the HAE binding pocket (by superimposition onto HAE) showing that the C6-hydroxyl group is not only well accommodated within the pocket but also possibly makes an additional hydrogen bonding connection to U2869. H bonds are represented as green dotted lines; π-stacking interactions are in pink.

(C) Acylation of the HAE C11-hydroxyl results in significant steric clashes with C2821 and U2873. Derivatization of the C11-hydroxyl results in structures that cannot be accommodated within the binding pocket, leading to the understanding of the previous IC_{50} inhibition data. Steric clashes are represented as red dotted lines.

(D) Bufanisine, which has the opposite stereochemistry at position 10b (Figure 4), is inactive most likely because it cannot be accommodated in the pocket as a result of a serious steric clash with U2873 (represented as red dotted lines).

cleft of the *S. cerevisiae* 25S rRNA when compared with *E. coli* 23S (PDB: 4YBB) (Figure S3B). Nonetheless, despite the overall similarity it has been previously shown that NAR does not bind to *E. coli* ribosomes (Baez and Vazquez, 1978) and its binding is unaffected by varying the concentration of [Mg^{2+}], [K^{+}], or the pH. Our analysis points out that the presence of a single rRNA substitution in the A-site cleft of bacteria, and precisely the replacement of a pyrimidine (U2822 in yeast) with a purine (A2453 in bacteria), is very likely to be responsible for HAE discrimination. This substitution would allow the conserved residue U2504 (U2873 in yeast) to adopt a different conformation and, ultimately, to sterically clash with HAE in the case of the prokaryotic ribosome (Figure S3B).

Based on the HAE/80S complex structure, and given the high structural similarity of the binding pocket between yeast and human 80S (Figure 3C), we can provide a thorough explanation of existing SAR data of HAE congeners, leading us to propose the mechanism by which these compounds might interact with, or be rejected from, the A-site cleft. This represents the first step toward the development of innovative crinine-based alkaloids as anticancer agents, which until now has been seriously hampered by the lack of structural information that could be used for rational design of superior analogs. We noticed, for instance, that HAD (Figures 4, 5A, and 5B) might create an additional H bond with the 25S rRNA, therefore explaining the slight increase in activity (Figure 4). In contrast, acylation of C11 (see Figure 4 for numbering) gives rise to inactive compounds, due to the steric clash that would occur between the acyl group and the 25S rRNA residues (Figures 5C and 5D). Our analysis also highlights the possible sites of functionalization of alkaloids, such as C3, which might generate a more potent compound due to the available volume that can accommodate different chemical groups and allow changes in stereochemistry. Another interesting site on alkaloids is C6, where the presence of an additional hydroxyl group slightly improves the potency of HAD thanks to the new interaction established with the 25S rRNA.

Compounds affecting protein synthesis globally are expected to also affect ribosome biogenesis simply because the process relies on numerous assembly factors and 80 ribosomal proteins that are translated by the ribosome in the cytoplasm. Moreover, since the PTC is composed only of rRNA (Polacek and Mankin, 2005) and since it is formed relatively early during subunit biogenesis, we reasoned that AA might also associate with subunit precursors, potentially interfering with assembly factor association and subunit biogenesis. The question we then asked was: do different classes of compounds exert specific effects on pre-rRNA processing? Our data showed that the addition of alkaloids (HAE, HAD, LYC, and NAR) to colon cancer cells stimulate the accumulation of the primary transcript 47S pre-rRNA (Figures 6 and S4). Furthermore, the compounds also exert an inhibitory effect on the processing of the 32S and 12S rRNA in ITS2, involved in the production of the mature 28S and 5.8S, which are constituents of the LSU (Figure S4). Importantly, these effects were not seen with CHX that also inhibits translation, hence demonstrating that AA-mediated processing inhibitions are highly specific.

An antitumor surveillance pathway has been described that provides a direct connection between failure of

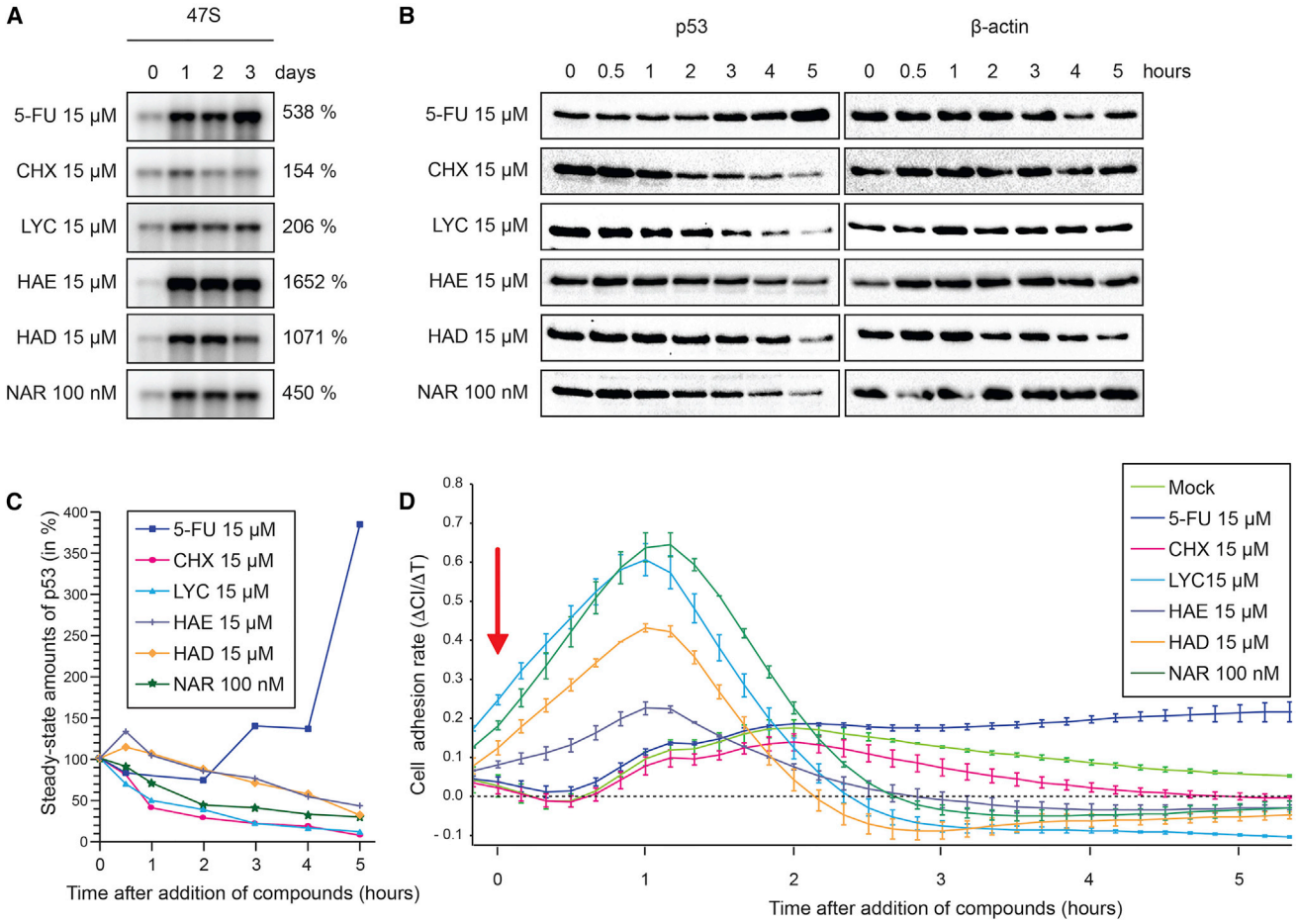

Figure 6. Effects of AAs on Ribosome Biogenesis and p53 Homeostasis

(A) Pre-rRNA processing analysis of the 47S precursor. Total RNA extracted from HCT116 cells treated with the indicated compound (concentration corresponding to their IC_{50}, see STAR Methods) in a time-course analysis for up to 3 days was analyzed by northern blotting. The membrane was probed with an oligonucleotide specific to the primary transcript (47S). Other pre-rRNA intermediates were detected with specific probes (see Figure S4A).

(B) Analysis of p53 steady-state accumulation. Total protein was extracted from HCT116 cells treated with the indicated compound in a time-course analysis for up to 5 hr and analyzed by western blotting. The blots were probed with an antibody specific to p53 or β-actin (control).

(C) Quantification of (B). The signal was quantified by luminescence with a ChemiDoc (Bio-Rad). Steady-state amounts of p53 are expressed as percentages of the level at time 0 hr.

(D) Real-time impedance measurements. The cell index (CI) was captured with an iCELLigence device (ACEA) in real time for up to 5 hr after addition of the drugs and expressed as a cell adhesion rate (ΔCI/ΔT). Red arrow points to the time of compound addition. 5-FU, 5-fluorouracil; CHX, cycloheximide; LYC, lycorine; HAE, haemanthamine; HAD, haemanthidine; NAR, narciclasine. All compounds were used at their IC_{50}. Data are presented as mean ± SEM.

See also Figures S4–S7.

ribosome biogenesis and p53-induced cell death (Golomb et al., 2014). We were therefore intrigued to learn whether AAs are able to induce such a p53 response. Western blotting experiments revealed that p53 protein is stabilized after addition of HAE or HAD to colon carcinoma cells. While in normal cells the constitutive degradation of p53 avoids activation of programmed cell death, its stabilization after addition of ribosome biogenesis inhibitors represents an effective and promising way to commit cancer cells to death (Bywater et al., 2012; Peltonen et al., 2014). Furthermore, we have shown here for 5-FU and HAE that the presence of p53 in cells is indeed required for the effect of nucleolar stress activation to be impactful on cell growth limitation (Figures 6 and S7).

In conclusion, the cytostatic effect of at least two AAs tested in this work (HAE and HAD) might not be due solely to their effect on protein synthesis (inhibition of mature, translating ribosomes, through binding to the A-site of the 60S subunit). It might additionally be the consequence of activation of nucleolar surveillance and consequent stabilization of p53, effects that we suggest are caused primarily by specific inhibition of pre-rRNA processing. Thus, by comparison with compounds that do not trigger a nucleolar stress response and p53 stabilization, HAE and HAD might prove advantageous in cancer therapy. As a clear perspective, we can envisage using the crystal structure of HAE in complex with the eukaryotic 80S ribosome for a computer-guided design of molecules that could potentially have enhanced

potencies and reduced toxicities after specific fine-tuning of their binding selectivities.

STAR★METHODS

Detailed methods are provided in the online version of this paper and include the following:

- KEY RESOURCES TABLE
- CONTACT FOR REAGENT AND RESOURCE SHARING
- EXPERIMENTAL MODEL AND SUBJECT DETAILS
  - Plant Cells
  - Yeast Cells
  - Human Cells
- METHOD DETAILS
  - Extraction and Purification of HAE
  - Ribosome Purification and Crystallization
  - Data Collection and Structure Determination
  - Human Cell Culture and Drug Treatment
  - Cell Adhesion Assays with iCELLigence
  - Western Blotting
  - Northern Blotting
  - Computational Analysis
  - Yeast Plate Assay
- QUANTIFICATION AND STATISTICAL ANALYSIS
- DATA AND SOFTWARE AVAILABILITY

SUPPLEMENTAL INFORMATION

Supplemental Information includes seven figures and can be found with this article online at https://doi.org/10.1016/j.str.2018.01.009.

ACKNOWLEDGMENTS

This work was supported by the French National Research Agency, ANR-15-CE11-0021-01 (to G.Y.), "Fondation ARC pour la Recherche sur le Cancer" (to G.Y.), "La Fondation pour la Recherche Médicale" DBF20160635745, France (to S.P. and G.Y.), European Research Council advanced grant 294312 (to M.M. and M.Y.), and the Russian Government Program of Competitive Growth of Kazan Federal University (to M.Y.). The Yusupov group is grateful to the staff of PROXIMA 1 beamline at the synchrotron SOLEIL (France) and, in particular, to Dr. Leonard Chavas and Dr. Pierre Legrand for providing rapid access and assisting with data collection. The lab of D.L.J.L. is supported by the Université Libre de Bruxelles (ULB), the Fonds National de la Recherche (F.R.S./FNRS), the Walloon Region (DGO6), the Fédération Wallonie-Bruxelles, and the European Research Development Fund (ERDF). A.K. acknowledges the NCI NIH grant CA186046. A.E. was supported by an academic grant from the University of Naples Federico II, Naples, Italy.

AUTHOR CONTRIBUTIONS

A.K., V.M., D.L.J.L., G.Y., and M.Y. designed the experiments and supervised the study; M.M. purified and crystallized the 80S ribosome sample; S.P. and M.M. collected the X-ray diffraction data; S.P. carried out data processing, structure determination, and interpretation of the HAE/80S structure; S.C.P. performed the docking studies; C.Z., S.A.B., and K.S. performed all the biochemical experiments concerning inhibition of ribosome biogenesis and induction of p53 signal; A.E. extracted and purified HAE and also supplied the HAD sample; S.P., V.M., D.L.J.L., and A.K. wrote the first draft of the manuscript, with input from all the authors.

DECLARATION OF INTERESTS

The authors declare no competing interests.

Received: October 3, 2017
Revised: December 1, 2017
Accepted: January 12, 2018
Published: February 8, 2018

SUPPORTING CITATIONS

The following references appear in the Supplemental Information: Mullineux and Lafontaine (2012).

REFERENCES

Afonine, P.V., Grosse-Kunstleve, R.W., Echols, N., Headd, J.J., Moriarty, N.W., Mustyakimov, M., Terwilliger, T.C., Urzhumtsev, A., Zwart, P.H., and Adams, P.D. (2012). Towards automated crystallographic structure refinement with phenix.refine. Acta Crystallogr. D Biol. Crystallogr. *68*, 352–367.

Al Ustwani, O., Griffiths, E.A., Wang, E.S., and Wetzler, M. (2014). Omacetaxine mepesuccinate in chronic myeloid leukemia. Expert Opin. Pharmacother. *15*, 2397–2405.

Baez, A., and Vazquez, D. (1978). Binding of [^{3}H]narciclasine to eukaryotic ribosomes. A study on a structure-activity relationship. Biochim. Biophys. Acta *518*, 95–103.

Ben-Shem, A., Garreau de Loubresse, N., Melnikov, S., Jenner, L., Yusupova, G., and Yusupov, M. (2011). The structure of the eukaryotic ribosome at 3.0 Å resolution. Science *334*, 1524–1529.

Berkov, S., Bastida, J., Sidjimova, B., Viladomat, F., and Codina, C. (2011). Alkaloid diversity in *Galanthus elwesii* and *Galanthus nivalis*. Chem. Biodivers. *8*, 115–130.

Bhat, M., Robichaud, N., Hulea, L., Sonenberg, N., Pelletier, J., and Topisirovic, I. (2015). Targeting the translation machinery in cancer. Nat. Rev. Drug Discov. *14*, 261–278.

Bruno, I.J., Cole, J.C., Kessler, M., Luo, J., Motherwell, W.D., Purkis, L.H., Smith, B.R., Taylor, R., Cooper, R.I., Harris, S.E., et al. (2004). Retrieval of crystallographically-derived molecular geometry information. J. Chem. Inf. Comput. Sci. *44*, 2133–2144.

Bywater, M.J., Poortinga, G., Sanij, E., Hein, N., Peck, A., Cullinane, C., Wall, M., Cluse, L., Drygin, D., Anderes, K., et al. (2012). Inhibition of RNA polymerase I as a therapeutic strategy to promote cancer-specific activation of p53. Cancer Cell *22*, 51–65.

Cedron, J.C., Ravelo, A.G., Leon, L.G., Padron, J.M., and Estevez-Braun, A. (2015). Antiproliferative and structure activity relationships of amaryllidaceae alkaloids. Molecules *20*, 13854–13863.

Chen, V.B., Arendall, W.B., Headd, J.J., Keedy, D.A., Immormino, R.M., Kapral, G.J., Murray, L.W., Richardson, J.S., and Richardson, D.C. (2010). MolProbity: all-atom structure validation for macromolecular crystallography. Acta Crystallogr. D Biol. Crystallogr. *66*, 12–21.

Donati, G., Peddigari, S., Mercer, C.A., and Thomas, G. (2013). 5S ribosomal RNA is an essential component of a nascent ribosomal precursor complex that regulates the Hdm2-p53 checkpoint. Cell Rep. *4*, 87–98.

Emsley, P., Lohkamp, B., Scott, W.G., and Cowtan, K. (2010). Features and development of Coot. Acta Crystallogr. D Biol. Crystallogr. *66*, 486–501.

Furst, R. (2016). Narciclasine—an amaryllidaceae alkaloid with potent anti-tumor and anti-inflammatory properties. Planta Med. *82*, 1389–1394.

Garreau de Loubresse, N., Prokhorova, I., Holtkamp, W., Rodnina, M.V., Yusupova, G., and Yusupov, M. (2014). Structural basis for the inhibition of the eukaryotic ribosome. Nature *513*, 517–522.

Golomb, L., Volarevic, S., and Oren, M. (2014). p53 and ribosome biogenesis stress: the essentials. FEBS Lett. *588*, 2571–2579.

Greber, B.J., Gerhardy, S., Leitner, A., Leibundgut, M., Salem, M., Boehringer, D., Leulliot, N., Aebersold, R., Panse, V.G., and Ban, N. (2016). Insertion of the biogenesis factor rei1 probes the ribosomal tunnel during 60s maturation. Cell *164*, 91–102.

Hohmann, J., Forgo, P., Molnár, J., Wolfard, K., Molnár, A., Thalhammer, T., Máthé, I., and Sharples, D. (2002). Antiproliferative amaryllidaceae alkaloids

isolated from the bulbs of *Sprekelia formosissima* and *Hymenocallis x festalis*. Planta Med. *68*, 454–457.

Hroch, M., Mičuda, S., Havelek, R., Cermanová, J., Cahlíková, L., Hošťálková, A., Hulcová, D., and Řezáčová, M. (2016). LC-MS/MS method for the determination of haemanthamine in rat plasma, bile and urine and its application to a pilot pharmacokinetic study. Biomed. Chromatogr. *30*, 1083–1091.

Ingrassia, L., Lefranc, F., Mathieu, V., Darro, F., and Kiss, R. (2008). Amaryllidaceae isocarbostyril alkaloids and their derivatives as promising antitumor agents. Transl. Oncol. *1*, 1–13.

Jimenez, A., Santos, A., Alonso, G., and Vazquez, D. (1976). Inhibitors of protein synthesis in eukaryotic cells. Comparative effects of some amaryllidaceae alkaloids. Biochim. Biophys. Acta *425*, 342–348.

Kabsch, W. (2010). Integration, scaling, space-group assignment and post-refinement. Acta Crystallogr. D Biol. Crystallogr. *66*, 133–144.

Könst, Z.A., Szklarski, A.R., Pellegrino, S., Michalak, S.E., Meyer, M., Zanette, C., Cencic, R., Nam, S., Voora, V.K., Horne, D.A., et al. (2017). Synthesis facilitates an understanding of the structural basis for translation inhibition by the lissoclimides. Nat. Chem. *9*, 1140–1149.

Kukhanova, M., Victorova, L., and Krayevsky, A. (1983). Peptidyltransferase center of ribosomes. On the mechanism of action of alkaloid lycorine. FEBS Lett. *160*, 129–133.

Lamoral-Theys, D., Andolfi, A., Van Goietsenoven, G., Cimmino, A., Le Calvé, B., Wauthoz, N., Mégalizzi, V., Gras, T., Bruyère, C., Dubois, J., et al. (2009). Lycorine, the main phenanthridine Amaryllidaceae alkaloid, exhibits significant antitumor activity in cancer cells that display resistance to proapoptotic stimuli: an investigation of structure-activity relationship and mechanistic insight. J. Med. Chem. *52*, 6244–6256.

Likhitwitayawuid, K., Angerhofer, C.K., Chai, H., Pezzuto, J.M., Cordell, G.A., and Ruangrungsi, N. (1993). Cytotoxic and antimalarial alkaloids from the bulbs of *Crinum amabile*. J. Nat. Prod. *56*, 1331–1338.

Lubbe, A., Gude, H., Verpoorte, R., and Choi, Y.H. (2013). Seasonal accumulation of major alkaloids in organs of pharmaceutical crop *Narcissus* Carlton. Phytochemistry *88*, 43–53.

Luchetti, G., Johnston, R., Mathieu, V., Lefranc, F., Hayden, K., Andolfi, A., Lamoral-Theys, D., Reisenauer, M.R., Champion, C., Pelly, S.C., et al. (2012). Bulbispermine: a crinine-type Amaryllidaceae alkaloid exhibiting cytostatic activity toward apoptosis-resistant glioma cells. ChemMedChem *7*, 815–822.

McClary, B., Zinshteyn, B., Meyer, M., Jouanneau, M., Pellegrino, S., Yusupova, G., Schuller, A., Reyes, J.C.P., Lu, J., Guo, Z., et al. (2017). Inhibition of eukaryotic translation by the antitumor natural product agelastatin A. Cell Chem. Biol. *24*, 605–613.e5.

Melnikov, S., Ben-Shem, A., Garreau de Loubresse, N., Jenner, L., Yusupova, G., and Yusupov, M. (2012). One core, two shells: bacterial and eukaryotic ribosomes. Nat. Struct. Mol. Biol. *19*, 560–567.

Mullineux, S.T., and Lafontaine, D.L. (2012). Mapping the cleavage sites on mammalian pre-rRNAs: where do we stand? Biochimie *94*, 1521–1532.

Myasnikov, A.G., Kundhavai Natchiar, S., Nebout, M., Hazemann, I., Imbert, V., Khatter, H., Peyron, J.F., and Klaholz, B.P. (2016). Structure-function insights reveal the human ribosome as a cancer target for antibiotics. Nat. Commun. *7*, 12856.

Nair, J.J., Bastida, J., Viladomat, F., and van Staden, J. (2012). Cytotoxic agents of the crinane series of amaryllidaceae alkaloids. Nat. Prod. Commun. *7*, 1677–1688.

Nicolas, E., Parisot, P., Pinto-Monteiro, C., de Walque, R., De Vleeschouwer, C., and Lafontaine, D.L. (2016). Involvement of human ribosomal proteins in nucleolar structure and p53-dependent nucleolar stress. Nat. Commun. *7*, 11390.

Nita, M.E., Nagawa, H., Tominaga, O., Tsuno, N., Fujii, S., Sasaki, S., Fu, C.G., Takenoue, T., Tsuruo, T., and Muto, T. (1998). 5-Fluorouracil induces apoptosis in human colon cancer cell lines with modulation of Bcl-2 family proteins. Br. J. Cancer *78*, 986–992.

Novac, O., Guenier, A.S., and Pelletier, J. (2004). Inhibitors of protein synthesis identified by a high throughput multiplexed translation screen. Nucleic Acids Res. *32*, 902–915.

Pabuççuoglu, V., Richomme, P., Gözler, T., Kivçak, B., Freyer, A.J., and Shamma, M. (1989). Four new crinine-type alkaloids from Sternbergia species. J. Nat. Prod. *52*, 785–791.

Pelletier, J., and Peltz, S.W. (2007). Therapeutic opportunities in translation. In Translational Control in Biology and Medicine, M.B. Mathews, N. Sonenberg, and J.W.B. Hershey, eds. (Cold Spring Harbor Laboratory Press), pp. 855–895.

Peltonen, K., Colis, L., Liu, H., Jaamaa, S., Zhang, Z., Af Hallstrom, T., Moore, H.M., Sirajuddin, P., and Laiho, M. (2014). Small molecule BMH-compounds that inhibit RNA polymerase I and cause nucleolar stress. Mol. Cancer Ther. *13*, 2537–2546.

Pestov, D.G., Strezoska, Z., and Lau, L.F. (2001). Evidence of p53-dependent cross-talk between ribosome biogenesis and the cell cycle: effects of nucleolar protein Bop1 on G(1)/S transition. Mol. Cell. Biol. *21*, 4246–4255.

Pettit, G.R., Melody, N., and Herald, D.L. (2004). Antineoplastic agents. 511. Direct phosphorylation of phenpanstatin and pancratistatin. J. Nat. Prod. *67*, 322–327.

Polacek, N., and Mankin, A.S. (2005). The ribosomal peptidyl transferase center: structure, function, evolution, inhibition. Crit. Rev. Biochem. Mol. Biol. *40*, 285–311.

Sener, B., Orhan, I., and Satayavivad, J. (2003). Antimalarial activity screening of some alkaloids and the plant extracts from Amaryllidaceae. Phytother. Res. *17*, 1220–1223.

Shibnath Ghosal, A., and Razdan, S. (1985). (+)-Epimaritidine, an alkaloid from *Zephyranthes rosea*. Phytochemistry *24*, 635–637.

Sloan, K.E., Bohnsack, M.T., and Watkins, N.J. (2013). The 5S RNP couples p53 homeostasis to ribosome biogenesis and nucleolar stress. Cell Rep. *5*, 237–247.

Strunk, B.S., Loucks, C.R., Su, M., Vashisth, H., Cheng, S., Schilling, J., Brooks, C.L., 3rd, Karbstein, K., and Skiniotis, G. (2011). Ribosome assembly factors prevent premature translation initiation by 40S assembly intermediates. Science *333*, 1449–1453.

Tafforeau, L., Zorbas, C., Langhendries, J.L., Mullineux, S.T., Stamatopoulou, V., Mullier, R., Wacheul, L., and Lafontaine, D.L.J. (2013). The complexity of human ribosome biogenesis revealed by systematic nucleolar screening of Pre-rRNA processing factors. Mol. Cell *51*, 539–551.

Truitt, M.L., and Ruggero, D. (2017). New frontiers in translational control of the cancer genome. Nat. Rev. Cancer *17*, 332.

Van Goietsenoven, G., Andolfi, A., Lallemand, B., Cimmino, A., Lamoral-Theys, D., Gras, T., Abou-Donia, A., Dubois, J., Lefranc, F., Mathieu, V., et al. (2010). Amaryllidaceae alkaloids belonging to different structural subgroups display activity against apoptosis-resistant cancer cells. J. Nat. Prod. *73*, 1223–1227.

Voorhees, R.M., Weixlbaumer, A., Loakes, D., Kelley, A.C., and Ramakrishnan, V. (2009). Insights into substrate stabilization from snapshots of the peptidyl transferase center of the intact 70S ribosome. Nat. Struct. Mol. Biol. *16*, 528–533.

Wilson, D.N. (2014). Ribosome-targeting antibiotics and mechanisms of bacterial resistance. Nat. Rev. Microbiol. *12*, 35–48.

Wu, S., Tutuncuoglu, B., Yan, K., Brown, H., Zhang, Y., Tan, D., Gamalinda, M., Yuan, Y., Li, Z., Jakovljevic, J., et al. (2016). Diverse roles of assembly factors revealed by structures of late nuclear pre-60S ribosomes. Nature *534*, 133–137.

STAR★METHODS

KEY RESOURCES TABLE

REAGENT or RESOURCE	SOURCE	IDENTIFIER
Antibodies		
Mouse monoclonal anti-beta actin, unconjugated, clone AC-15	Santa Cruz Biotechnology	Cat#sc-69879; Lot#C0315; RRID:AB_1119529
Mouse monoclonal anti-p53, unconjugated, clone DO-1	Santa Cruz Biotechnology	Cat#sc-126; Lot#I231; RRID:AB_628082
Mouse monoclonal anti-GAPDH, unconjugated, clone GAPDH-71.1	Sigma-Aldrich	Cat#G8795; RRID:AB_1078991
Rabbit polyclonal anti-SP1, unconjugated	Merck	Cat#07-645; RRID:AB_310773
Goat polyclonal anti-mouse IgG-HRP	Jackson ImmunoResearch Labs	Cat#115-036-062; Lot#128842; RRID:AB_2307346
Donkey polyclonal anti-rabbit IgG-HRP	Santa Cruz Biotechnology	Cat#sc-2313; RRID:AB_641181
Chemicals, Peptides, and Recombinant Proteins		
5-Fluorouracil	Sigma	Cat#F-6627
Cycloheximide	Sigma	Cat#C-1988
Deposited Data		
Crystal structure of HAE/80S complex	PDB, This study	5ON6
Experimental Models: Cell Lines		
Homo sapiens, HCT116 p53+/+	ATCC	Cat#CCL-247
Homo sapiens, HCT116 p53-/-	Tafforeau et al., 2013	N/A
Experimental Models: Organisms/Strains		
Narcissus pseudonarcissus King Alfred	*Jacques Amand International, Ltd nurseries in Middlesex, England.*	N/A
Saccharomyces cerevisiae, strain background JD1370	Ben-Shem et al., 2011	N/A
Saccharomyces cerevisiae, BY4741	Euroscarf	Cat#Y00000
Oligonucleotides		
Northern blot probe LD1844 (5'-ETS): CGGAGGCCCAACCTCTCCGACGACAGGTC GCCAGAGGACAGCGTGTCAGC	Tafforeau et al., 2013	N/A
Northern blot probe LD1827 (ITS-1): CCTCGCCCTCCGGGCTCCGTTAATGATC	Tafforeau et al., 2013	N/A
Northern blot probe LD1828 (ITS-2):CTGC GAGGGAACCCCCAGCCGCGCA	Tafforeau et al., 2013	N/A
Software and Algorithms		
Maestro release 2017-3	Schrodinger	https://www.schrodinger.com/
XDS	Kabsch, 2010	http://xds.mpimf-heidelberg.mpg.de
XDSCONV	Kabsch, 2010	http://xds.mpimf-heidelberg.mpg.de/html_doc/xdsconv_program.html
phenix.refine	Afonine et al., 2012	https://www.phenix-online.org/
MarvinSketch	ChemAxon	http://www.chemaxon.com
Grade web server	Global Phasing	http://grade.globalphasing.org
Coot	Emsley et al., 2010	https://www2.mrc-lmb.cam.ac.uk/personal/pemsley/coot/
Mogul	Bruno et al., 2004	https://validate-rcsb-1.wwpdb.org
PyMOL 1.7.4	The PyMol Molecular Graphics System, Version 1.7.4.0	Schrodinger, LLC
Molprobity	Chen et al., 2010	http://molprobity.biochem.duke.edu
RTCA Data Analysis Softare 1.0	ACEA Biosciences	N/A

CONTACT FOR REAGENT AND RESOURCE SHARING

Further information and requests for resources and reagents should be directed to and will be fulfilled by the Lead Contact, Denis L.J. Lafontaine (denis.lafontaine@ulb.ac.be).

EXPERIMENTAL MODEL AND SUBJECT DETAILS

Plant Cells

Narcissus pseudonarcissus var. *King Alfred* was used to extract haemanthamine.

Yeast Cells

Yeast cells used for ribosome purification: strain JD1370. Yeast cells used for testing sensitivity towards haemanthamine: strain BY4741 (*Saccharomyces cerevisiae*, Euroscarf). Yeast cells were cultured in complete medium (yeast extract/peptone/dextrose) at 30°C.

Human Cells

Human cells used for growth assays, ribosome biogenesis analysis, and nucleolar surveillance activation: colon carcinoma cells HCT116 p53 +/+ and HCT116 p53 -/- (*Homo sapiens*, adult male, ATCC). The cell lines used in this work were obtained directly from ATCC and passaged in the laboratory for fewer than 6 months after receipt. All cell lines were diagnosed by short tandem repeat (STR) profiling by ATCC. HCT116 cells were cultured in McCoy medium (Lonza) supplemented with 10% Fetal Bovine Serum (Sigma) and 1% penicillin-streptomycin (Gibco) at 37°C.

METHOD DETAILS

Extraction and Purification of HAE

Six kilograms of dried bulbs of *Narcissus pseudonarcissus* var. *King Alfred* were extracted with a Soxhlet using petroleum ether for 24 h and then MeOH for 72 h. The MeOH extract (903.6 g) was purified by flash chromatography using the mixture EtOAc:MeOH:H_2O (85:10:5 v/v/v) as eluent. The fractions containing HAE were eluted with a step of CH_2CL_2-MeOH 8:2 (v/v) and combined, concentrated and HAE was collected as an amorphous solid (2.7 g, 465 mg/kg). HAE was identified by comparing its ^{1}H NMR data and optical rotation with those reporting in literature (Pabuççuoglu et al., 1989; Shibnath Ghosal and Razdan, 1985). The purity of the samples was confirmed by TLC, mp, optical rotation, ^{1}H and ^{13}C NMR, NOESY, and ESI-MS analyses (Luchetti et al., 2012).

Ribosome Purification and Crystallization

80S ribosomes from the yeast *S. cerevisiae* were purified to homogeneity (Ben-Shem et al., 2011). Crystals were grown at 4 °C by hanging-drop vapor diffusion and cryo-protected as previously described (Ben-Shem et al., 2011; Garreau de Loubresse et al., 2014), keeping the glycerol concentration at a constant concentration of 20% through all the steps. Crystals reached their maturity after 4-5 weeks of drops equilibration. The HAE/80S ribosome complex was formed by soaking the compound, at a final concentration of 1 mM, with the pre-formed 80S ribosome crystals for 1.5 hours at 4 °C in the final step of crystals treatment, as described (Garreau de Loubresse et al., 2014). Crystals were then harvested and frozen directly on the cryo-stream prior to plunging into liquid N_2.

Data Collection and Structure Determination

Data were collected at SOLEIL synchrotron, beamline PROXIMA1 at cryogenic temperature, using a Pilatus-6M detector. Low dose data were collected from several crystals at a wavelength (λ) of 1.148 Å, corresponding to a nominal energy of 10.8 keV. Fully redundant diffraction data were collected and, after processing, the intensities scaled using the XDS suite (Kabsch, 2010), to a maximum resolution of 3.1 Å. The resulting file was converted into mtz format (XDSCONV program) and then submitted for a first cycle of rigid body refinement in phenix.refine (PHENIX suite, (Afonine et al., 2012)) by taking each chain as a single rigid body. As initial model we used the *Saccharomyces cerevisiae* vacant 80S ribosome (PDB ID: 4V88). Positive difference density map (F_{obs} - F_{calc}) was then manually inspected for the presence of the inhibitor, which was placed unambiguously (Figure S1). Electron density for haemanthamine was observed only at a single binding site. Drawing of the chemical structure was performed using the MarvinSketch suite (ChemAxon, http://www.chemaxon.com/). Coordinates and restraints for HAE were generated online with the Grade web server (Global Phasing, http://grade.globalphasing.org). Ligand fitting and remodeling of the ribosomal binding pocket was performed manually using Coot (Emsley et al., 2010). Further cycles of individual coordinates, TLS restraints and grouped isotropic B-factor refinement were performed using phenix.refine, yielding the crystallographic statistics presented in Table 1. HAE geometry was validated with the software Mogul (Bruno et al., 2004), as implemented in the wwPDB validation server (https://validate-rcsb-1.wwpdb.org). All the figures of the crystal structure were prepared with PyMOL 1.7.4 (Schrödinger,

http://pymol.org). Structure validation was performed using Molprobity (Chen et al., 2010) and resulted in the following Ramachandran plot distribution: 88.00% favored, 11.00% allowed and 1.00% outliers. The structure has been deposited at PDB (accession number 5ON6).

Human Cell Culture and Drug Treatment

HCT116 cells were seeded into 6-well plates at 2-6x10^5 cells per well. After approximately 24 hours, the medium was removed and replaced with fresh complete growth medium supplemented with the indicated drug for the indicated incubation time. Fresh stock solutions of haemanthamine, haemanthidine, narciclasine, lycorine, cycloheximide (Sigma, C-1988), and 5-fluorouracil (Sigma, F-6627) were dissolved in dimethyl sulfoxide (DMSO, Sigma). For cell treatment with each drug, the stock solutions were diluted with the complete growth medium to working concentrations ensuring that the DMSO concentration did not exceed 0.1%. Control cells were treated with 0.1% DMSO only.

Cell Adhesion Assays with iCELLigence

Cell adhesion was monitored by means of real-time electric impedance measurements and captured as a cell index (CI) with the RTCA iCELLigence System. Cell adhesion reflects cell attachment to the growth support, which depends on cell proliferation and cell morphology. 150 μl McCoy's complete medium was added to each well of L8 E-plates and the plates were fitted on the iCELLigence reader in a 37°C incubator with 5% CO_2 to obtain background readings. 325 μl of 'HCT116 p53 +/+' and 'HCT116 p53 -/-' cell suspensions containing 6x10^4 cells was added to each well and the E-plates were placed on the iCELLigence station in the incubator. The cell index was monitored every 10 minutes with the iCELLigence system. Approximately 24 hours later, while the cells were still in the exponential growth phase, the plates were removed from the incubator and compounds (25 μl of 20x fresh dilutions) were added to the wells containing the cells (0-h time points on the graphs). Plates were placed on the iCELLigence reader in the incubator and the electrical impedance was measured every 10 minutes for 120 hours. The cell adhesion rate ($\Delta CI/\Delta T$) was plotted as a function of time.

Western Blotting

30 μg total protein extract was resolved on a 10% Tris/glycine SDS-polyacrylamide gel and transferred onto a PVDF membrane according to the manufacturer's instructions. The membranes were blocked for 1 hour at RT with Tris-buffered saline (TBS) supplemented with 0.1% Tween-20 (TBS-T) and 5% milk. Membranes were incubated with primary antibodies overnight at 4°C with shaking. The primary antibodies used were 1:1,000 anti β-actin (Santa Cruz, SC69879), 1:10,000 anti-GAPDH (Sigma, G8795), 1:2,500 anti-Sp1 (Merck 07-645), and 1:1,000 anti-p-53 (Santa Cruz, SC126) diluted in TBS-T/3% milk. The membranes were washed three times with TBS-T and incubated with shaking for 2 h at RT with secondary antibody coupled with HRP (anti-mouse IgG-HRP, Jackson ImmunoResearch, 115-036-062, or anti-rabbit IgG-HRP, Santa Cruz, SC2313) diluted in TBS-T/3% milk. The membranes were washed three times in TBS-T and incubated in SuperSignal West Pico Chemiluminescent Substrate (Thermo Scientific) for 5 min before imaging with a ChemiDoc MP system (Biorad).

Northern Blotting

Total RNA extracted (5μg) from HCT116 cells, after addition of alkaloids, was resolved on a denaturing agarose gel (6% formaldehyde, 1.2% agarose in buffer containing 50 mM HEPES and 1 mM EDTA). Electrophoresis was carried out for 16 h at 65V at RT in HEPES/EDTA buffer. RNA transfer by capillarity from agarose gels onto Hybond-N^+ membranes was carried out overnight in 10x saline–sodium citrate. The membranes were prehybridized for 1 h at 65°C in 50% formamide, 5x SSPE, 5x Denhardt's solution, 1% (wt/vol) SDS, and 200 μg/ml fish sperm DNA solution (Roche). The primary transcript (47S) and all major pre-rRNA intermediates were detected with specific probes: a P^{32}-labelled oligonucleotide probe was added and incubated for 1 h at 65°C and then overnight at 37°C. The probes used were (indicated in Figure S4): LD1844: 5'- CGGAGGCCCAACCTCTCCGACGACAGGTCGCCAGAGGACAGCGTGTCAGC-3'; LD1827; 5'- CCTCGCCCTCCGGGCTCCGTTAATGATC-3'; LD1828: 5'- CTGCGAGGGAACCCCCAGCCGCGCA-3'. Fuji imaging plates (Fujifilm) were exposed to Northern blots. The signals were acquired with a Phosphorimager (FLA-7000; Fujifilm) and quantified with the native MultiGauge software (Fujifilm, v 3.1).

Computational Analysis

The structure of HAE in complex with the eukaryotic 80S ribosome was visualized using the Biovia Discovery Studio visualizer. The structures of bulbispermine, HAD, acylated HAE and bulbispermine methiodide were created in Discovery Studio visualizer and superimposed onto the HAE structure, allowing for rationalization of the observed SAR data.

Yeast Plate Assay

Serial dilutions of exponentially growing wild-type yeast cells, strain BY4741 (used as wild-type reference by the Euroscarf consortium), were spotted on rich medium supplemented or not with haemanthamine (HAE) and incubated for 3 days at 30°C. The complete medium was prepared with yeast extracts from two suppliers independently: MP (cat ref. 103303) and Formedium (cat ref. YEA03).

QUANTIFICATION AND STATISTICAL ANALYSIS

Details regarding statistical and experimental replicates can be found within the Method Details section and/or the corresponding figure legends where appropriate.

DATA AND SOFTWARE AVAILABILITY

The atomic coordinates and structure factors for the reported crystal structure have been deposited in the Protein Data Bank under accession code 5ON6.

Structure, Volume *26*

Supplemental Information

The Amaryllidaceae Alkaloid Haemanthamine Binds the Eukaryotic Ribosome to Repress Cancer Cell Growth

Simone Pellegrino, Mélanie Meyer, Christiane Zorbas, Soumaya A. Bouchta, Kritika Saraf, Stephen C. Pelly, Gulnara Yusupova, Antonio Evidente, Véronique Mathieu, Alexander Kornienko, Denis L.J. Lafontaine, and Marat Yusupov

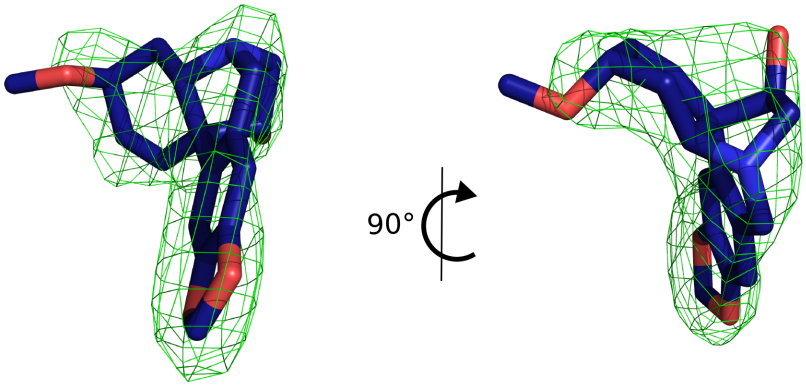

Figure S1: Density quality allow us to unambiguously determine HAE position and binding mode. Related to Figure 2. Unbiased F_{obs} - F_{calc} electron density map issue of the first cycle of rigid-body refinement using the vacant *S. cerevisiae* 80S structure (PDB ID: 4V88) as starting model. The map (represented as green meshes) includes only the HAE compound, it is contoured at 3σ and is represented in two views, 90° apart.

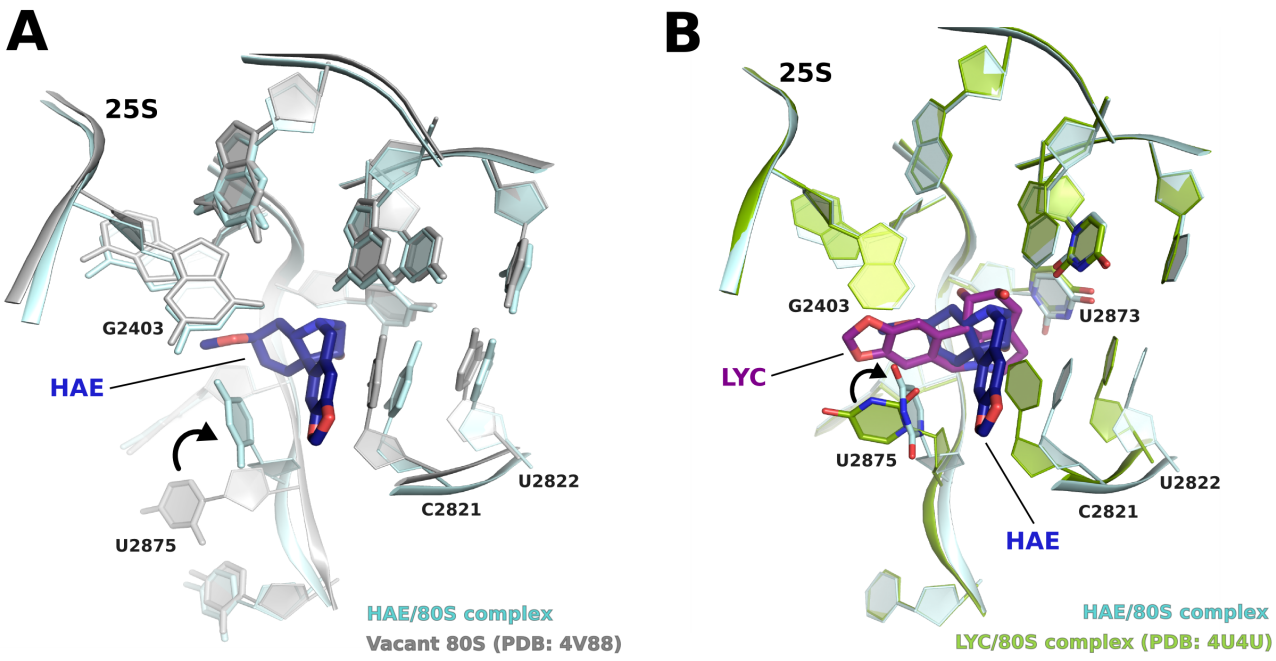

Figure S2: Rearrangement of the A-site cleft on the 25S rRNA is inhibitor dependent. Related to Figure 3. (A) Superposition of the A-site cleft of vacant yeast 80S ribosome (PDB ID: 4V88) with our structure. We can observe that residues C2821 and U2822 are displaced upon accommodation of the inhibitor, likely driven by hydrophobic forces that push them away from the PTC, as seen in the case of NAR/80S structure (PDB ID: 4U51). The "flip-up" movement of residue U2875, not observed for other alkaloids before, is significant and likely induces further stabilization of the HAE in the A-site cleft. (B) Superposition based on the LSU of the HAE/80S A-site cleft (this work) with the LYC/80S complex previously published (PDB code: 4U4U). Although the binding pocket is constituted by the same residues and the compounds share chemical structure similarity, the interactions network is remarkably different.

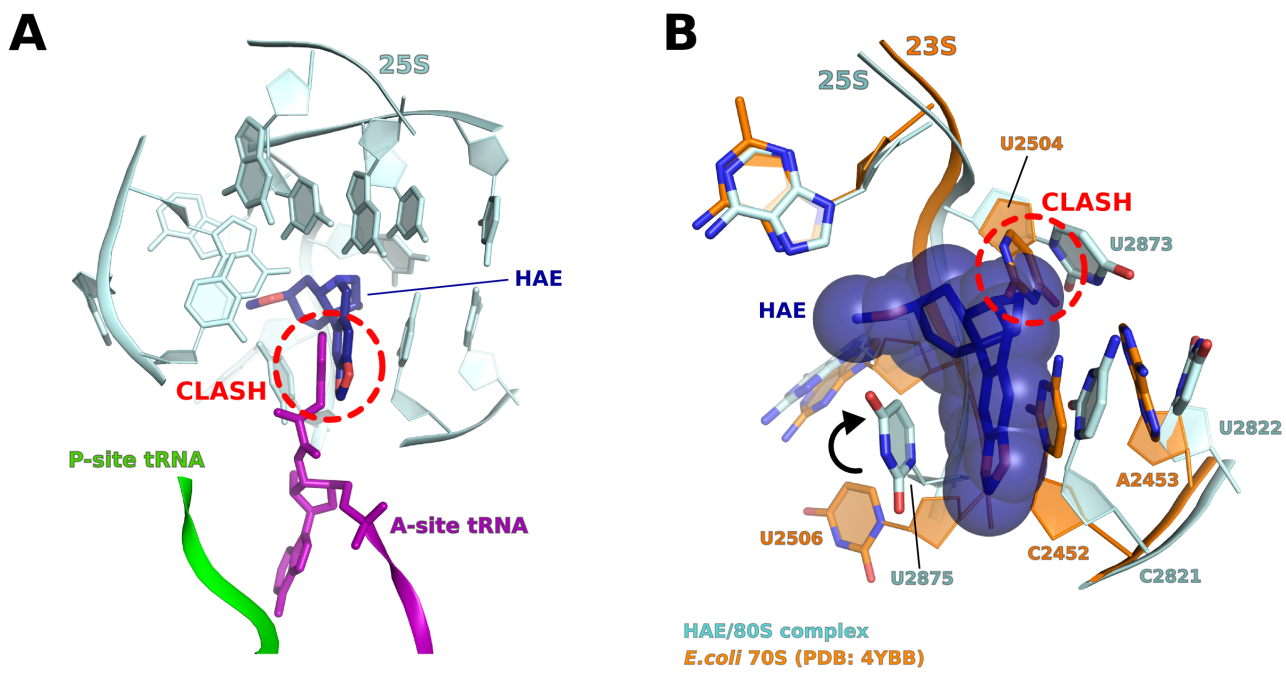

Figure S3: HAE is an eukaryotic specific inhibitor and its binding is predicted to clash with the newly coming A-site tRNA. Related to Figure 3. (A) *In silico* model of an actively translating 80S ribosome. Aminoacylated A- and P-site (amino acid not shown for clarity) tRNAs are taken from the 70S structure of *T. thermophilus* (PDB ID: 4V5D), after superposition of the *S. cerevisiae* 25S rRNA with the bacterial 23S rRNA. The steric clash that would occur upon HAE binding to the A-site cleft is highlighted in red. HAE will impair the accommodation of any long-chain or bulky amino acid in the A-site cleft, thus blocking the elongation phase of translation. (B) Superposition of the 25S rRNA A-site cleft of the HAE/80S complex with the *E. coli* vacant 23S rRNA structure (PDB ID: 4YBB). We can observe several rearrangements of the rRNA residues in the pocket. Although some displacements are very similar to what has been detected in the vacant *S. cerevisiae* 80S structure (Fig. S2A), precisely concerning the movement of the C2452 and U2506 (C2821 and U2875 in yeast, respectively), the analysis pinpoints the likely candidate in charge of discriminate the inhibitor's binding between the two kingdoms. The residue U2504 (U2873 in yeast) is adopting a different conformation in the bacterial A-site cleft, as a consequence of the presence of a purine (instead of a pyrimidine) close to the conserved C2452 (C2821 in yeast). The conformation of U2504 would then sterically clash with the inhibitor, likely rejecting its binding to the pocket and making it inefficient for interaction with the bacterial ribosome.

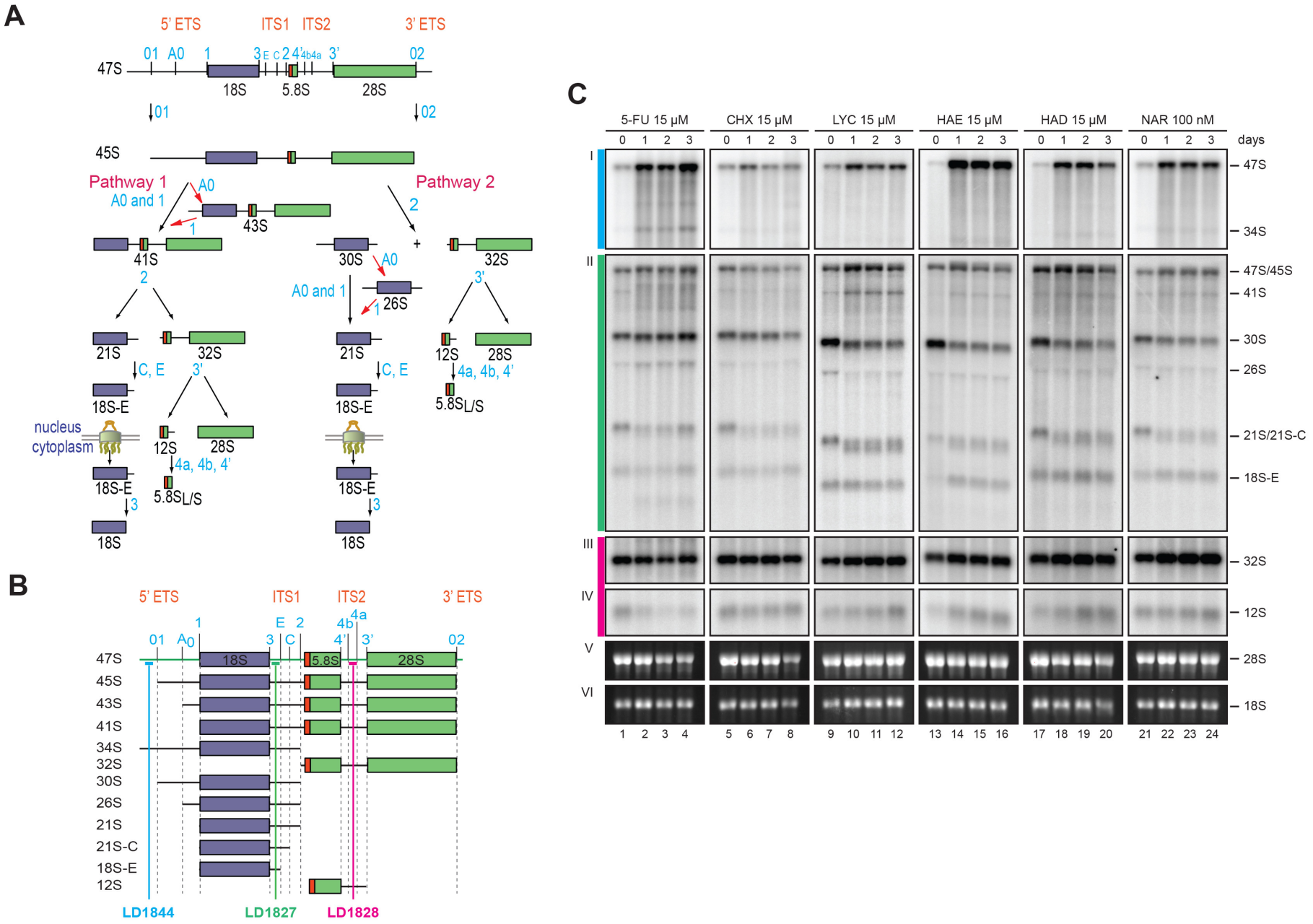
A
5' ETS
ITS1
ITS2
3' ETS
01
A0
1
3
E
C
2
4'
4b
4a
3'
02
47S
18S
5.8S
28S
45S
Pathway 1
A0 and 1
Pathway 2
43S
41S
30S
32S
26S
21S
C, E
3'
18S-E
12S
28S
4a, 4b, 4'
5.8S L/S
nucleus
cytoplasm
18S
B
LD1844
LD1827
LD1828
21S-C
C
5-FU 15 µM
CHX 15 µM
LYC 15 µM
HAE 15 µM
HAD 15 µM
NAR 100 nM
days
I
II
III
IV
V
VI
47S
34S
47S/45S
41S
30S
26S
21S/21S-C
18S-E
32S
12S
28S
18S

Figure S4: Effects of *Amaryllidaceae* alkaloids on pre-rRNA processing in cultured cancer cells. Related to Figure 6. (A) Pre-rRNA processing pathway in human cells and major pre-rRNA intermediates (see Mullineux and Lafontaine, 2012 for details). Three of the four mature rRNAs, the 18S, 5.8S, and 28S rRNAs are produced from a single RNA Pol I transcript (47S). The 18S rRNA is the RNA component of the small subunit (40S); 5.8S and 28S are incorporated into the large subunit (LSU, 60S). There is a third rRNA in the 60S subunit, 5S, which is independently produced by RNA Pol III (not shown). The mature sequences are embedded in noncoding 5' and 3' external transcribed spacers (ETS) and internal transcribed spacers (ITS1 and 2). Cleavage sites (in cyan) and alternative pathways are indicated (pathways 1 and 2). For details, see Www.RibosomeSynthesis.Com. (B) Northern blot probes used in this work (LD1844, LD1827, and LD1828) highlighting the pre-rRNA species detected. (C) Northern blot analysis. Total RNA extracted from HCT116 cells treated with the indicated *Amaryllidaceae* alkaloid for 1, 2, or 3 days was resolved on denaturing gels and analyzed by Northern blotting with specific probes (see panel B). As controls, cells were treated with 5-FU or CHX. Remarkably, the pre-rRNA processing inhibitions observed with the four AAs are highly similar (e.g. 32S accumulation and 21S/21S-C and 18S-E accumulation only seen in AA-treated cells). Furthermore, the AA processing inhibitions are highly specific as they are strikingly different to those observed with the control compounds (5-FU and CHX: reduced 32S and no effect on 32S, respectively, and no particular effects on 21S/21S-C or 18S-E). Blots were probed with oligonucleotide LD1844 (panel I), LD1827 (panel II), or LD1828 (panels III and IV). Panels V and VI show ethidium-bromide-stained gels.

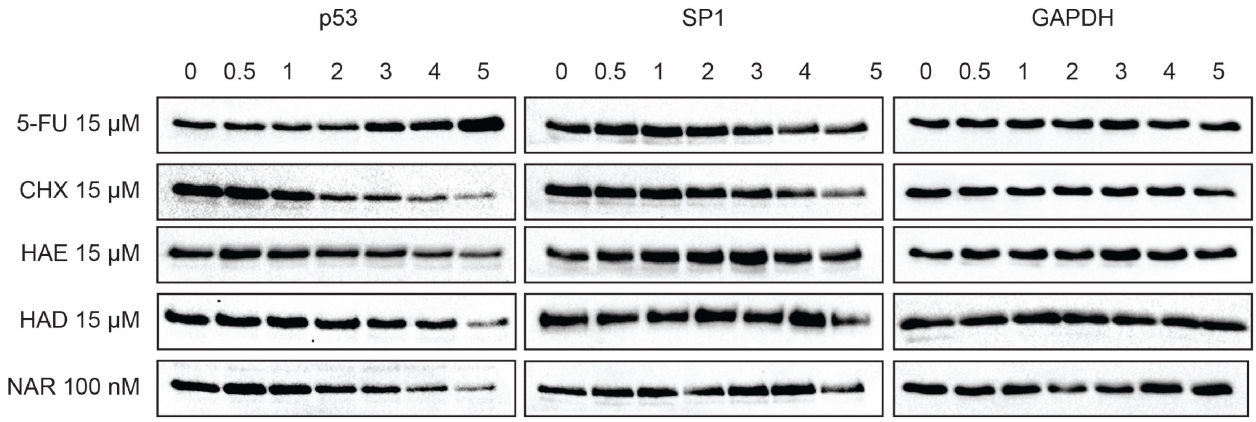

Figure S5: Effects of *Amaryllidaceae* alkaloids on p53 homeostasis. Related to Figure 6. Analysis of p53 steady-state accumulation. The figure shows the same samples as those presented in Fig. 6B with the blots probed for additional loading controls (SP1 and GAPDH). Total protein was extracted from HCT116 cells treated with the indicated compound in a time-course analysis for up to 5 hours and analysed by Western blotting. The blots were probed with an antibody specific to p53, SP1, or GAPDH (control).

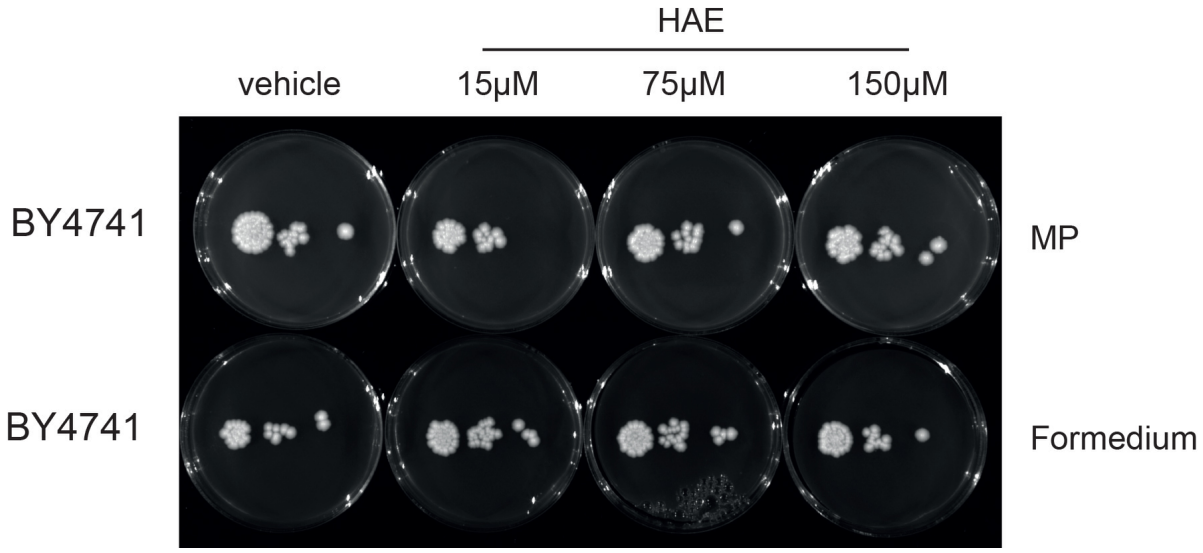

Figure S6: Yeast cells are not sensitive to haemanthamine. Related to Figure 6. The data show that yeast cells are not sensitive to HAE even at concentration 10 times higher than those used on human cells. The wild-type strain used is the Euroscarf consortium wild-type BY4741. From left to right: vehicle alone (DMSO 0.15%), HAE 15 μM, HAE 75 μM, and HAE 150 μM. The complete medium was prepared with yeast extracts from two suppliers as we previously observed that yeast extract origin may influence drug sensitivity. Top raw: yeast extract from MP; bottom raw: yeast extract from Formedium (STAR Methods). The results are the same with both yeast extracts.

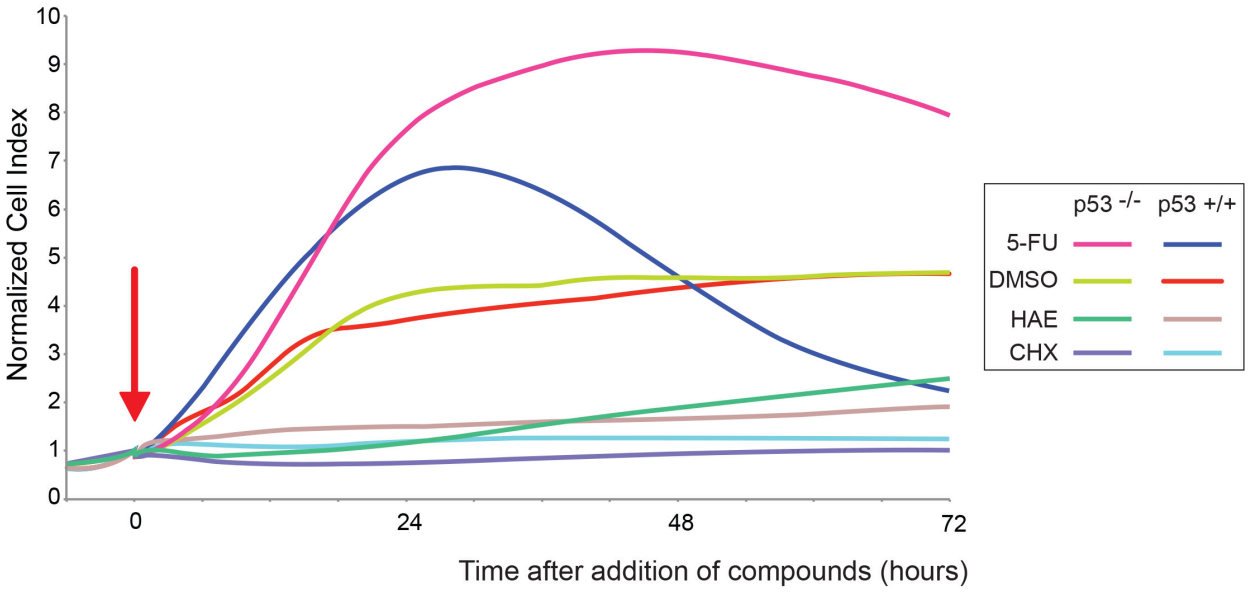

Figure S7: The effects on cancer cell proliferation of compounds that activate nucleolar stress (5-FU and HAE) require the presence of p53 in cells. Related to Figure 6. Two isogenic diploid human cancer cell lines, one expressing p53 (HCT116 p53 +/+) and one not expressing p53 (HCT116 p53 -/-), were seeded on gold-plated multi-well plates, treated with the indicated compounds, and cell proliferation monitored by real-time impedance measurements for 3 days. The growth of cells treated with 5-FU declines more rapidly and more sharply in cells that express p53 (navy blue profile) than in cells that do not express p53 (in pink). Similarly, the cell growth is more inhibited upon HAE treatment in cells that express p53 (in brown) than in cells that do not express p53 (dark green). In contrast, treatment of cells with CHX, which does not activate nucleolar stress, inhibits growth similarly in presence (cyan) or absence (purple) of p53 (i.e. parallel profiles). As control, cells treated with the drug vehicle alone (DMSO) grow similarly irrespective of their p53 status: the light green and red profiles are similar (red, HCT116 p53 +/+; light green, HCT116 p53 -/-). All compounds were used at 15 μM and added after 1 day of growth (0-hr time point, red arrow). The results are expressed as normalized cell index. The experiment was performed in duplicate, the mean is shown.